Received: 2 October 2021 | Revised: 15 February 2022 | Accepted: 17 May 2022

DOI: 10.1002/we.2755

RESEARCH ARTICLE

WILEY

Fatigue design sensitivities of large monopile offshore wind turbines

Stian H. Sørum[1,2] | George Katsikogiannis[2] | Erin E. Bachynski-Polić[1,2] | Jørgen Amdahl[1,2] | Ana M. Page[3] | Rasmus T. Klinkvort[3]

[1]Centre for Autonomous Marine Operations and Systems, Department of Marine Technology, NTNU, Trondheim, Norway

[2]Department of Marine Technology, NTNU, Trondheim, Norway

[3]Norwegian Geotechnical Institute, Oslo, Norway

Correspondence
Stian H. Sørum, NTNU, NO-7491 Trondheim, Norway.
Email: stian.h.sorum@ntnu.no

Funding information
Research Council of Norway, Grant/Award Number: 223254; Extra Large Monopiles (WAS-XL), Grant/Award Number: 268182

Abstract

The input for fatigue analyses of offshore wind turbines is typically chosen based on design values provided by design standards. While this provides a straightforward design methodology, the contribution of different input parameters to the uncertainty in the fatigue damage estimates is usually unknown. This knowledge is important to have when improving current designs and methodologies, and the parameters governing the uncertainty is typically found through a sensitivity analysis. Several sensitivity studies have been performed for monopile-based offshore wind turbines, typically focusing on specific turbines and engineering disciplines. This paper performs a sensitivity study for three monopile-based offshore wind turbines (5 MW, 10 MW, 15 MW) using parameters from several engineering disciplines. The results show that the fatigue utilization is primarily governed by the uncertainty in the SN curves and fatigue capacity. Following this, the uncertainty in the environmental conditions is the dominating uncertainty, with wind loads becoming increasingly important as turbine size increases. Additionally, the effect of modelling uncertainties is investigated. The wind-related model uncertainties dominate in the tower top, while uncertainties in the wave and soil models dominate in the tower base and monopile. Designers wanting to reduce the uncertainty in a design are recommended to focus on the environmental conditions, and using as accurate models as possible. All modelling uncertainties are significant, but research should particularly be focused on wave directionality and soil models.

KEYWORDS
design uncertainty, fatigue design, model uncertainty, offshore wind turbine, sensitivity analysis

1 | INTRODUCTION

Fatigue limit state (FLS) design of offshore wind turbines (OWTs) is based on design load cases according to relevant design standards.[1,2] These standards account for the uncertainty in resistance and loads by applying safety factors to achieve a specified reliability level. The procedure is straightforward for designers, but safety factors give no information on how the uncertainty in specific variables influences the overall reliability

of an OWT. Such knowledge is essential for improving current design standards, reducing investment costs, evaluating novel design concepts, and guiding further research.

Although all design parameters may in principle be considered uncertain, typically only a few parameters significantly affect the total uncertainty.[3] These parameters should be given particular focus during the design process, and they can be identified through a sensitivity analysis (SA). Numerous SAs and reliability studies have been performed on individual OWTs,[4–14] with size varying from 4 to 10 MW. The results from selected studies considering several uncertain parameters are summarised in Table 1. None of the studies have directly compared different turbine sizes. Many of these have considered a limited number of design parameters, while others are more extensive.[4–6,8,10,11] Others again have focused on uncertainties from selected engineering disciplines, for example, aerodynamics.[9,11] However, there is no clear consensus between the

TABLE 1 Selected previous sensitivity analyses for monopile OWTs

Reference	Hübler et al.[5]	Robertson et al.[9]	Toft et al.[11]	Teixeira et al.[8]	Peeringa &Bedon[4]	Velarde et al.[6]
Turbine size (MW)	5	5	-	5	4	10
Turbulence intensity	NI	I	I	I		
Wind shear	NI	I	NI	NI		
Surface roughness				NI		
Air density	NI		NI	NI		
Air stability				NI		
Wind speed	V			V		
Wind direction	V					
Yaw error	NI	I		NI		
Water depth	NI			NI		
Water density	NI			NI		
Wave height	V			V		
Wave period	V			V		
Spectral parameter, γ				NI		
Wave direction	V					
Current velocity				NI		
Mass coefficient					NI	
Drag coefficient					NI	
Marine growth	I					
Wave load model						I
Soil stiffness	NI				NI	
Soil unit weight	I					
Soil friction angle	I					
Pile diameter	I					
Pile thickness	NI					
Tower diameter	NI					
Tower thickness	NI					
Embedded length	I					
Airfoil parameters		I				
Young's modulus	NI				NI	
SCF						NI
SN-curve					I	NI
Fatigue capacity					I	I
Dynamics						I
Hub mass	NI					
Nacelle mass	NI					

Note: "I"/green and "NI"/yellow denote parameters found influential and not influential, respectively. "V"/grey denotes parameters where the long-term variability is considered, as discussed in Section 4.1.3. Only important parameters from Robertson et al. are included.

studies regarding either the parameters considered, or the parameters identified as important. This may be caused both by different sensitivities for different turbines and foundations, as well as by the level of uncertainty assumed in the studies. Further, several studies overestimate the uncertainty in environmental conditions by considering the long-term variation in, for example, significant wave height rather than the uncertainty in the design value. An example of how this artificially increases the uncertainty is given in Section 4.1.3. Finally, some studies suggest further research topics without quantifying the uncertainty.[15,16]

The approaches followed by the studies in Table 1 differ. Hübler et al[5] focused on parameters from several engineering disciplines, looking at a large number of variables (>100). Robertson et al[9] performed a sensitivity analysis for 57 parameters, all related to wind characteristics and aerodynamic loads. For brevity, only the influential parameters from this study are included in Table 1. Toft et al[11] presented a probabilistic framework for assessment of the structural reliability level of wind turbines in fatigue loading, focusing on aerodynamic loads. Teixeira et al[8] performed a probabilistic sensitivity analysis including aerodynamic loads, wave conditions, and current velocity. Peeringa et al[4] presented a probabilistic design tool, coupling reliability analysis and wind turbine simulation tools, focusing on structural properties and fatigue capacity. Finally, Velarde et al[6] demonstrated a fatigue reliability analysis of a monopile supporting a 10-MW offshore wind turbine, focusing more on the system properties than the fundamental parameters. Three of the six studies in Table 1 found turbulence intensity to be important. Besides this, the SN curve was the only parameter found important by more than one study.

Beyond the uncertainty in design parameters, the modelling choices made in the analysis of an OWT introduce additional, different uncertainties. Several studies have been performed looking at individual parameters; some are given here to illustrate the range of model uncertainties. Kim et al[17] showed how wake effects increase the fatigue damage. Nybø et al[18] investigated the fatigue response using different wind fields and stability conditions, also comparing the engineering models with wind measurements and high-fidelity models of the wind field. Horn et al[19] and Schløer et al[20] found that higher order wave loads increase the fatigue damage in severe sea states. Horn et al[21] looked at the importance of considering multiple wave directions. They found that separation between wind generated waves and swell increased the monopile fatigue damage and reduced the tower fatigue damage. Including short-crested waves was found to reduce the fatigue damage. Sørum et al[22] showed that short-crested waves may result in both a higher and lower fatigue damage than long-crested waves, depending on the monopile design. Bachynski and Ormberg[23] showed that wave diffraction becomes more important as monopile diameters increase. Finally, Aasen et al[24] and Katsikogiannis et al[25] both demonstrated how the soil model influences the fatigue response predictions, with both nonlinear stiffness and damping being important. To the authors' knowledge, no studies compare the uncertainty caused by modelling choices to other types of uncertainty.

This paper aims to improve the understanding obtained from previous studies, focusing on fatigue design for three monopile-based OWTs with capacity 5, 10, and 15 MW. A sensitivity analysis study is first performed considering the input parameters whose uncertainty can be described by a continuous probability density function, hereafter denoted continuous parameters. The uncertainty in fatigue damage estimates due to modelling choices, hereafter denoted discrete parameters, is then calculated. The studied parameters range across various engineering disciplines, including but not limited to aerodynamics, hydrodynamics, geotechnics, and structural dynamics. The present work aims to determine which uncertainties contribute most to the uncertainty in fatigue damage for different locations along the support structure and operational states for monopile-based OWTs, and how this uncertainty varies with turbine size. The results can help designers prioritise which parameters to investigate during the design of turbines and give guidance for the focus of further research.

The paper is organized as follows: Section 2 presents the sensitivity analysis method used in the study; Section 3 describes the environmental model, simulation models and fatigue estimation method. Following this, Section 4 presents the parameters investigated in the SA. Finally, the results are presented in Section 5 and discussed in Section 6, before the paper is concluded in Section 7.

2 | SENSITIVITY ANALYSIS METHODS

Different methods can be used for a sensitivity analysis,[3] depending on the system properties and the computational effort required. The design of monopile OWTs relies on dynamic analyses, coupling aerodynamics, hydrodynamics, soil–structure interaction and the turbine control system. The system is nonlinear, and the computational effort required for analysis is significant with simulations running at approximately real-time. Local analyses, such as one-at-the-time (OAT) variation of the input parameters, are computationally efficient but not capable of capturing system nonlinearities and interactions between input parameters. Variance-based methods provide more accurate results, allowing quantification of each parameter's influence on the system's total uncertainty. However, the large computational effort of variance-based methods makes them infeasible to apply here. Screening methods can partly overcome the challenges mentioned above, capture system nonlinearities, interaction effects, and qualitatively rank the input parameters according to their importance, with acceptable computational requirements. In this study, the screening method of elementary effects is used for evaluating the continuous parameters (see Section 2.1). The method is generally considered a good alternative for highly nonlinear systems with a moderate (<100) number of input parameters.[3] The discrete parameters are evaluated based on the change relative to a baseline model, as described in Section 2.2.

2.1 | Elementary effects method

The elementary effects method is an expansion of the OAT approach, as illustrated in Figure 1. The quantity of interest (i.e. long term fatigue damage) is calculated at a base point j that represents a set of input values for the uncertain analysis parameters (e.g., turbulence intensity and yaw error). A single parameter is then changed, and the quantity of interest is calculated again. The local derivative, denoted the elementary effect (*EE*), can then be found. The procedure is repeated for several sets of base points distributed across the parameter space. The output quantity, Y, is a function of all input parameters, $\mathbf{X} = [X_1, X_2, ..., X_I]^T$. The EE of an input parameter X_i, at a base point $j = 1, ..., J$, is given by Equation (1).

$$EE_i^j = \frac{Y(X_1^j, ..., X_i^j \pm \Delta_i, ..., X_I^j) - Y(X_1^j, ..., X_i^j, ..., X_I^j)}{\pm \Delta_F} = \frac{Y_{pp}^j - Y_{bp}^j}{\pm \Delta_F}. \quad (1)$$

$Y(X_1^j, ..., X_i^j, ..., X_I^j) = Y_{bp}^j$ is the output quantity calculated at the base point j, while $Y(X_1^j, ..., X_i^j \pm \Delta_i, ..., X_I^j) = Y_{pp}^j$ is the output quantity calculated for a specified perturbation Δ_i of input parameter X_i in the physical space. Δ_F is the normalised step size (Section 2.1.1). The sign of the perturbation is randomly selected. The importance of a parameter X_i is determined based on the statistics of all elementary effects across the J base points.

2.1.1 | Sampling strategy

The parameter space of each input variable should be sufficiently covered to achieve reliable results. It has been found that a radial elementary effect is more efficient than the original approach[26] if the sampled sets $\mathbf{X}^j$ are sufficiently distributed. Three main sampling approaches have been identified in the literature.[27–29] The first is Crude Monte Carlo methods, which show inadequate coverage of the parameter space.[28,29] Stratified approaches (e.g., Latin Hypercube) are more efficient but do not provide sufficient multidimensional coverage.[29] Finally, quasi-random sequences (e.g., Sobol and Hammersley) show better multidimensional properties.[27,28] A method for combining Hammersley sequences and Latin Hypercube sampling has also been developed.[29] The drawback of Latin Hypercube sampling is that the number of sampling points cannot be easily expanded if convergence is not met. Therefore, the quasi-random Sobol sequences were used in this study.

It is recommended to perform the input parameter sampling for EE analyses from a uniformly distributed sampling space,[3] denoted the **U**-space. This is achieved by mapping the set of input parameters, **X**, from the physical space (X-space), to uncorrelated uniformly distributed variables, **U**, based on Equation (2).

$$X_i = F_i^{-1}(U_i). \quad (2)$$

Here, F_i^{-1} is the inverse cumulative distribution function (CDF) of X_i, and U_i is an independent stochastic variable uniformly distributed in the range [0,1]. This sampling method ensures an appropriate concentration of base points at the most probable regions of the parameter space for each variable.

Finally, the step sizes in the physical and uniformly distributed space, Δ_i and Δ_F, are defined. The step size in the physical space is given implicitly by the transformation in Equation (2) and is expressed by Equation (3)

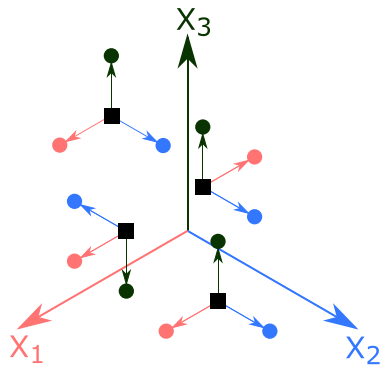

FIGURE 1 Illustration of the radial elementary effects method for three parameters ($I = 3$) and four base points ($J = 4$). The squares correspond to the base points, while the circles are the perturbed points. Adopted from Campolongo et al[26] and Robertson et al.[9]

$$X_i \pm \Delta_i = F_i^{-1}(U_i \pm \Delta_F). \tag{3}$$

In some studies,[26] the step size is treated as a random variable while other studies[9] use a fixed Δ_F with a random sign. The latter approach is adopted in the present work. To select the step size, it shall be ensured that Δ_F is sufficiently large to give a measurable change in the quantity of interest between the base point realisation $Y^j_{bp}(\mathbf{X})$ and the perturbed realisation $Y^j_{pp}(\mathbf{X})$. Additionally, it is desirable that the resultant step size Δ_i ensures an approximately linear variation between $Y^j_{bp}(\mathbf{X})$ and $Y^j_{pp}(\mathbf{X})$. $\Delta_F = 0.1$ was used here, as it gives measurable changes in $Y(\mathbf{X})$, while it is assumed to be small enough to ensure approximate linearity.

2.1.2 | Identification of important parameters

The quantity of interest for the sensitivity analysis in the present study is the long-term fatigue damage, denoted as D_{LT}. Therefore, the *EE* formulation from Equation (1) is now expressed as

$$EE^j_i = \frac{D_{LT}(X^j_1,\ldots,X^j_i \pm \Delta_i,\ldots,X^j_I) - D_{LT}(X^j_1,\ldots,X^j_i,\ldots,X^j_I)}{\pm\Delta_F}. \tag{4}$$

Several locations along the OWT support structure are considered, as different parameters may be important at different locations. The locations used are the tower top, tower base and seafloor, in addition to the location corresponding to the maximum monopile fatigue damage in each turbine. Identification of important parameters is done via evaluation of the absolute mean, $\mu^*_{EE,i}$, and variance, $\sigma^2_{EE,i}$, of the EE related to each input parameter:

$$\mu^*_{EE,i} = \frac{1}{J}\sum_{j=1}^{J} |EE^j_i|, \tag{5}$$

$$\sigma^2_{EE,i} = \frac{1}{J-1}\sum_{j=1}^{J} (EE^j_i - \mu_i)^2. \tag{6}$$

High $\mu^*_{EE,i}$ indicates an important parameter, while a large $\sigma_{EE,i}$ indicates coupling with other parameters. The mean, μ_i, in Equation (6) is defined as

$$\mu_i = \frac{1}{J}\sum_{j=1}^{J} EE^j_i. \tag{7}$$

2.2 | Discrete analysis method

The discrete parameters varied in this study are the wind coherence model, inclusion/exclusion of wave spreading, variation of wave spectral models and soil models, as well as inclusion/exclusion of scour protection in the structural model. These variations cannot be described by a probability density function (PDF), and the effect of discrete parameter variations are evaluated based on the change in fatigue damage compared to the baseline case (see Section 4.2). Only one discrete parameter is varied at a time, meaning that interactions between discrete parameters are not captured. However, the discrete analyses are repeated for all J base points from the continuous simulations. Interactions with the continuous parameters can therefore be captured. The relative change in fatigue damage is calculated as

$$\delta D^j_i = \frac{|D^{BL}_{LT}(\mathbf{X^j}) - D^{Var\ i}_{LT}(\mathbf{X^j})|}{D^{BL}_{LT}(\mathbf{X^j})}. \tag{8}$$

$D^{BL}_{LT}(\mathbf{X^j})$ is the long-term fatigue damage using the baseline model at realization j of the continuous parameters. $D^{Var\ i}_{LT}(\mathbf{X^j})$ is the long-term fatigue damage when using alternative model i.

The effect of changing each model is evaluated based on the absolute mean, $\mu^*_{\delta D,i}$, and variance, $\sigma^2_{\delta D,i}$, of the relative change in fatigue damage:

$$\mu^*_{\delta D,i} = \frac{1}{J}\sum_{j=1}^{J} |\delta D^j_i|, \tag{9}$$

$$\sigma^2_{\delta D,i} = \frac{1}{J-1}\sum_{j=1}^{J}\left(\delta D_i^j - \mu_{LT,i}\right)^2. \tag{10}$$

As for the continuous parameters, a high $\mu^*_{\delta D,i}$ indicates an important parameter. A high $\sigma_{\delta D,i}$ means there is a significant coupling between discrete model i and the continuous parameters. The mean, μ_i, in Equation (10) is defined as

$$\mu_{\delta D,i} = \frac{1}{J}\sum_{j=1}^{J}\delta D_i^j. \tag{11}$$

3 | MODEL DESCRIPTION

This section summarises the simulation models, turbine and foundation properties, load models and all relevant information for fatigue damage calculation.

3.1 | Turbine models

Three turbine models have been used in the study; the NREL 5 MW,[30] the DTU 10 MW[31] and the IEA 15 MW[32] reference wind turbines. The simulation models are based on the reference wind turbines, supported by different monopile foundations. The 5-MW foundation is based on the OC3 monopile[33] and the 10-MW foundation is based on Velarde and Bachynski.[34] The 15-MW tower is based on the original design,[32] while the monopile is designed for a target natural period below 5.5 s and verified using the method in Katsikogiannis et al.[35] Each of the three turbines applies its corresponding controller: the NREL Baseline Wind Turbine Controller,[30] the Basic DTU Wind Energy Controller[36] and NREL's Reference OpenSource Controller,[37] respectively. The turbines are assumed located at 30 m water depth on the Norwegian Continental Shelf, at (55.11°N, 3.47°E). Soil conditions at the site are assumed to consist of an idealized clay profile with linearly increasing undrained shear strength and parabolic variation of shear modulus with depth. Both operational and parked conditions are considered, using the same environmental conditions. Details of the key parameters of the different turbines are given in Table 2, while an illustration of the models is shown in Figure 2.

TABLE 2 Key parameters of the NREL 5 MW, DTU 10 MW and IEA 15 MW reference wind turbines including foundation

Parameter	Unit	NREL	DTU	IEA
Rated power	MW	5	10	15
Rated wind speed	m/s	11.4	11.4	10.59
Rated rotor speed	rpm	12.1	9.6	7.56
Hub height	m	90	119	150
Rotor diameter	m	126	178.3	240
RNA mass	tonnes	350	674	1017
Tower top diameter	m	3.87	6.25	6.54
Tower base diameter	m	6.00	9.18	9.96
Tower top wall thickness	m	0.025	0.035	0.024
Tower base wall thickness	m	0.035	0.063	0.036
Monopile diameter	m	7	9	11
Monopile wall thickness	m	0.07	0.11	0.11
Embedded length	m	28	36	44
1st fore-aft natural period[a]	s	3.9	3.6	5.3

[a]Using mean value of uncertain parameters, see Table 3.

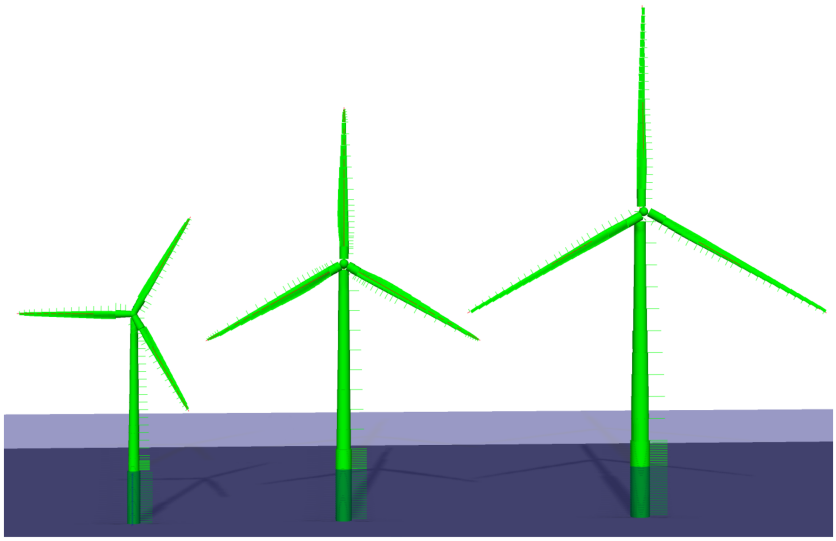

FIGURE 2 Illustration of the three SIMO-RIFLEX models in SIMA. From left to rigth: NREL 5 MW, DTU 10 MW and IEA 15 MW. The models are to scale, illustrating the size differences between the turbines

3.2 | Environmental model

Several numerical hindcast models are available for the northeast Atlantic Ocean. For the present study, the Norwegian Reanalysis Archive (NORA10)[38] hindcast data have been used. The database has 3-h resolution for the years 1957 to 2017 at the site, and provides information about met-ocean parameters such as mean wind speed 10 m above sea level, significant wave height (H_s), wave peak period (T_p) and wind-wave directionality.

To limit computational requirements, only three wind bins ($N_U = 3$) were considered: Close to the rated speed (8–10 m/s), intermediate (14–16 m/s) and high (20–22 m/s) wind speeds. The wave climate is assumed dependent on wind speed through the use of representative sea-state parameters (H_s - T_p) for each wind bin, based on the lumping method described by Katsikogiannis et al.[35] A Pierson–Moskowitz wave spectrum is used at the lowest wind speed, and a JONSWAP spectrum is used for the two higher wind speeds. The wind direction is assumed independent of other environmental parameters, while the wind-wave misalignment is assumed conditional on the wind speed.[48] The probability of an environmental condition at a base point j is given by Equation (12).

$$P^j(U_k, \theta_{wi}, \theta_{rel,m}) = P_n^j(U_k) \cdot P^j(\theta_{wi}) \cdot P_n^j(\theta_{rel,m}|U_k). \tag{12}$$

$P_n^j(U_k)$ is the frequency of occurrence of wind bin k, normalised to a total value of 1 based on Equation (13).

$$P_n^j(U_k) = \frac{P^j(U_k)}{\sum_{k=1}^{N_U} P^j(U_k)}. \tag{13}$$

$P^j(\theta_{wi})$ is the probability of occurrence of the wind direction, and $P_n^j(\theta_{rel,m}|U_k)$ is the conditional probability of the wind-wave misalignment. Two misalignment angles ($N_{\theta_{rel}} = 2$) were considered for each wind bin, 0° (aligned wind-waves) and 30°. Similarly to wind speed, the probability of the wind-wave misalignment angle for each wind bin is normalised to a sum of 1 as follows:

$$P_n^j(\theta_{rel,m}|U_k) = \frac{P^j(\theta_{rel,m}|U_k)}{\sum_{m=1}^{N_{\theta_{rel}}} P^j(\theta_{rel,m}|U_k)}. \tag{14}$$

The values of $P^j(U_k)$, $P^j(\theta_{wi})$ and $P^j(\theta_{rel,m}|U_k)$ are found by integrating the probability distributions given in Section 4.1 between the lower and upper limits for each bin considered. Two seed variations have been used for each environmental condition, to capture stochastic variations in the wind and wave loads.

3.3 | Simulation models

The rotor-nacelle assembly, tower and monopile above seabed were modelled in the aero-hydro-servo-elastic simulation tool SIMO-RIFLEX developed by SINTEF Ocean.[49,50] Structural components above seafloor are modelled as linear-elastic beam elements. The monopile part below seabed (foundation model) is described in detail in Section 3.4. The incoming wind field is generated using the program TurbSim from NREL[51] for the Kaimal spectrum and exponential coherence model, and IEC Turbulence Simulator from DTU for the Mann turbulence model.[52]

3.4 | Foundation model

The foundation model is a nonlinear macroelement model formulated within elastoplasticity theory. Macroelement models condense the response of the foundation and surrounding soil to a force-displacement relation at seafloor, separating the foundation and the rest of the structure.[53] The macroelement model has been developed to reproduce the nonlinear load-displacement response and the hysteretic damping of monopile-based OWTs in integrated time-domain analyses.[54–56] The basic features and limitations of the model are presented by Page et al.[55]

The macroelement model used in this study accounts for the change of the foundation stiffness due to nonlinear hysteretic soil behaviour, and as a consequence reproduces hysteretic damping. The model also accounts for the effect of multi-directional loading, which has been found to affect the foundation stiffness and hysteretic damping.[56] The model is calibrated to results of full 3D continuum modelling of the soil volume and the foundation by FEA. Even though the model have been calibrated to an idealized clay profile the results are equally valid for monopiles installed in sand. The importance here is the effect of the monopile head stiffness and how this influences the integrated analysis. The model communicates with SIMO-RIFLEX through a dynamic link library (DLL). The macroelement model does not directly compute the forces along the monopile below seabed, and a separate postprocessing numerical tool has been employed for that purpose. The tool is based on beam on spring model where the springs are calibrated to the results of the FEA using the methodology presented in Klinkvort et al.[57]

3.5 | Load models

Aerodynamic loads on the blades are calculated using blade element momentum theory with the Glauert induction and Prandtl tip loss corrections,[58] as well as dynamic stall and dynamic wake corrections. Hydrodynamic excitation loads are calculated using linear wave kinematics and MacCamy and Fuchs formulation[59] with Morison type drag. The hydrodynamic added mass is assumed to be constant, corresponding to an added mass coefficient $C_A = 1.0$.

3.6 | Fatigue damage estimation

Fatigue damage is estimated based on the axial stress in the monopile and tower. Individual stress cycles are identified using the rainflow counting technique implemented in the WAFO toolbox,[60] modified to allow for bi-linear S-N curves. The fatigue damage is calculated using Miner's sum[43] with thickness effects included. DNV GLs fatigue curve "D" for steel in sea water with cathodic protection was used for the monopile, while curve "D" for steel in air was selected for the tower.[43] The short-term fatigue utilization is calculated according to Equation (15).

$$D_{ST} = \frac{1}{\Delta_C} \sum_{i=1}^{n_\sigma} \frac{(\Delta\sigma_i)^{m_i}}{a_i} \left(\frac{t}{t_{ref}}\right)^{km_i}. \tag{15}$$

D_{ST} is the fatigue damage obtained from 1-h time-domain realisation for each environmental condition, Δ_C is the fatigue capacity and $\Delta\sigma_i$ are the individual stress ranges. m_i and a_i are the fatigue exponent and SN localisation parameters associated with each stress range. Finally, t is the wall thickness, t_{ref} is the reference wall thickness, and k is the thickness exponent on fatigue strength. A reference thickness equal to 25 mm and a thickness exponent of 0.2 were used.[43] The long-term fatigue damage, D_{LT}, is found by combining the short-term fatigue damage with the probability of occurrence for the associated environmental conditions.

4 | PARAMETERS FOR SENSITIVITY ANALYSIS

The selection of parameters for the sensitivity analysis is partly based on previously performed studies. In addition, some parameters have been added at the authors' discretion, while a limited number of parameters have been excluded due to the capabilities of the utilized simulation

software. For the continuous parameters, this selection is based on the studies in Table 1. Discrete parameters are selected based on studies on individual parameters.

4.1 | Continuous parameters

16 continuous parameters are considered in the SA, shown in Table 3. Details for the selected parameters are given in the following sections. A distinction from the distributions used in many previous studies is that the uncertainty in the design values for environmental conditions has been used. This approach is expected to give a more accurate prediction of the sensitivities than considering the short-term variability ("V" in Table 1, illustrated in Section 4.1.3). Where appropriate, the distributions are truncated 3 standard deviations above/below the mean to avoid nonphysical realizations.

4.1.1 | Wind speed

The uncertainty in the design wind speed is modelled as uncertainty in the parameters of a two-parameter Weibull distribution. Using 60 years of hindcast data from the NORA10 database,[38] a two-parameter Weibull distribution was fitted to the yearly data. This corresponds to assuming one year of measurements is available for the design, as required by design guidelines.[45] The uncertainty in the shape (α) and scale (β) parameters was assessed, and the scale parameter was found to be most important for variations in the fitted distribution. Only the scale parameter was treated as a stochastic variable, as it is desirable to limit the number of input parameters for the SA. A normal distribution was fitted to the scale parameter, while the shape parameter was taken as the value found from the fitted distribution to the full 60 years of data. The probability of occurrence for each wind speed bin is found based on Equation (16), while Table 4 summarises the wind speed distribution parameters used for the 10-MW turbine in the study. Values for the 5- and 15-MW turbines are extrapolated assuming the mean wind shear profile (Section 4.1.3).

TABLE 3 Distribution of continuous parameters considered for the sensitivity analysis

Parameter (X_i)	Symbol	Distribution	Section	Reference
Wind speed	U	-	Section 4.1.1	NORA10[38]
Wind direction	θ_{wi}	-	Section 4.1.2	NORA10[38]
Turbulence intensity	TI	-	Section 4.1.3	FINO1[39]
Wind shear	α	N(0.14,0.01)	Section 4.1.3	FINO1[39]
Yaw error	γ_Y	N(0°, 1°)	Section 4.1.4	Veldkamp[13]
Significant wave height	H_s	-	Section 4.1.5	NORA10[38]
Peak period	T_p	-	Section 4.1.5	NORA10[38]
Wind-wave misalignment	θ_{rel}	-	Section 4.1.6	NORA10[38]
Marine growth	t_{mg}	N(100 mm, 35 mm)	Section 4.1.7	Jusoh & Wolfram[40]
Drag coefficient	C_d	N(0.7,0.1)	Section 4.1.7	Peeringa & Bedon,[4] Veldkamp[13]
Undrained shear strength	s_u/σ'_{v0}	N(1,0.15)	Section 4.1.8	Lacasse & Nadim[41]
Void ratio	e	N(0.7,0.058)	Section 4.1.8	Lacasse & Nadim[41]
Monopile diameter	D_p	U(0.999μ, 1.001μ)	Section 4.1.9	Zaaijer,[42] Hübler et al.[5]
SN parameters	$\log(a_{1,2})$	-	Section 4.1.10	DNV GL[43]
Fatigue capacity	Δ_C	LN(1,0.3)	Section 4.1.10	Folsø et al.,[44] Peeringa&Bedon[4]
Unavailability	A	LN(0.1,0.025)	Section 4.1.11	DNV GL,[45] Pfaffel et al.,[46] Larsen et al.[47]

Note: -: Not described by a single distribution. N(μ,σ): Normal distribution mean μ and standard deviation σ. LN(μ,σ): Log-normal distribution mean μ and standard deviation σ. U(X_l,X_u): Uniform distribution with lower and upper limits X_l, X_u.

TABLE 4 Wind speed distribution parameters at 119 m above sea level

Parameter	Type	Distribution/value
Scale parameter, β	Stochastic	N(12.62,0.51)
Shape parameter, α	Deterministic	2.32

$$P^j(U_k;\alpha,\beta^j) = F_{wi}(U_{k,u};\alpha,\beta^j) - F_{wi}(U_{k,l};\alpha,\beta^j). \tag{16}$$

$F_{wi}(x;\alpha,\beta)$ is the Weibull CDF, U_k is the mean wind speed of bin k, while $U_{k,l}$, and $U_{k,u}$ are the lower and upper limits of the wind bin k. Superscript j represents the value of the stochastic variables at a base point j.

4.1.2 | Wind direction

Wind direction is treated similarly as the wind speed, with the uncertainty of the long-term distribution being modelled as variations in the distribution parameters. An individual distribution is fitted to each year in the NORA10 dataset. The probability of occurrence of a wind direction is found in Equation (17).

$$P^j(\theta_{wi}) = \int_{\theta_l}^{\theta_u} f(\theta_{wi};\mu,\kappa,\omega)d\theta_{wi}. \tag{17}$$

$f(\theta_{wi};\mu,\kappa,\omega)$ is the PDF of the wind direction, with θ_l, θ_u the lower and upper limits of the directionality bins. A three-mode von Mises mixture distribution is fitted to the yearly data.[61] Adopting the notation from Masseran et al,[61] the PDF of the distribution is expressed by Equation (18).

$$f(\theta_{wi};\boldsymbol{\mu},\boldsymbol{\kappa},\boldsymbol{\omega}) = \sum_{h=1}^{H} \omega_h \frac{1}{2\pi I_0(\kappa_h)} e^{\kappa_h \cos(\theta_{wi}-\mu_h)}. \tag{18}$$

Here, θ_{wi} is the wind direction in radians, while μ_h, κ_h and ω_h denote the mean direction, the concentration factor, and the weighting factor of each mode h, respectively.[61] The fitted PDF accounting for all years in the NORA 10 database is shown in Figure 3.

The variation in the fitted parameters was evaluated, and no correlation was observed. To limit the number of variables, only the mean values of the second and third modes were considered as stochastic variables. Both follow a normal distribution, as given in Table 5. The variation of the mean values is thus assumed to be representative of the uncertainty in the wind direction model.

With mode 1 being fixed, it is assumed that changing the mean of mode 2 and 3 towards a direction aligned with mode 1 (towards 58°) will increase the lifetime fatigue damage. Assuming mode 2 and 3 are related by

$$F_{\mu_3} = 1 - F_{\mu_2} \tag{19}$$

will ensure that mode 2 and 3 are either both more aligned with or more perpendicular to mode 1. This allows for representing the uncertainty in wind direction as one uncertainty in the two coupled parameters. However, the coupling is also likely to introduce overestimation of the

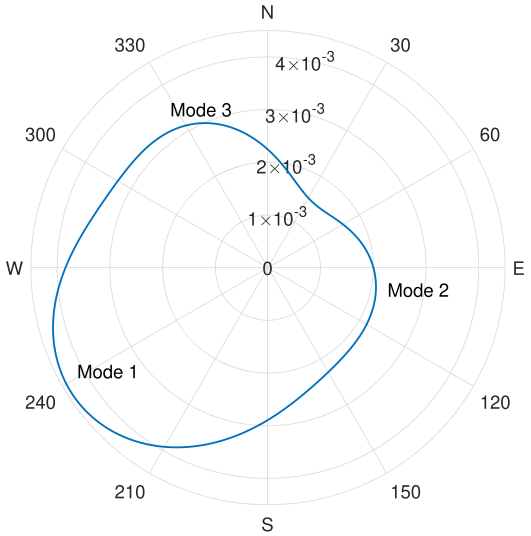

FIGURE 3 Fitted wind direction distribution for all years in NORA10 database

TABLE 5 Wind direction distribution parameters

Parameter	Type	Distribution/Value
μ_1	Deterministic	238°
μ_2	Stochastic	N(100°, 28.4°)
μ_3	Stochastic	N(333°, 43.3°)
κ_1	Deterministic	1.29
κ_2	Deterministic	1.10
κ_3	Deterministic	3.47
ω_1	Deterministic	0.598
ω_2	Deterministic	0.261
ω_3	Deterministic	0.142

Note: The uncertainty in the wind direction is modelled by the variations in μ_2 and μ_3.

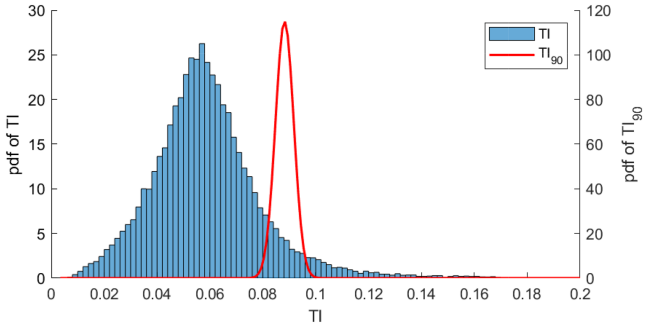

FIGURE 4 Distribution of 10-min turbulence intensity (*TI*) and design turbulence intensity (TI_{90})

importance of wind direction, as the fatigue damage may change more than if μ_2 and μ_3 were uncoupled. It should also be noted that the wind direction distribution also influences the wave direction, as the wave direction is modelled implicitly by the relative wind-wave direction in Section 3.2. The uncertainty in the wind-wave misalignment is treated separately in Section 4.1.6.

4.1.3 | Turbulence intensity and wind shear

The turbulence intensity and wind shear are assessed using 15 years of measurements from the FINO1 platform.[39] For turbulence intensity, the data from the topmost anemometer, 100 m above mean sea level (MSL), are used. To avoid wake effects from the nearby alpha ventus wind farm, only measurements from the westerly direction (180–360°) are used. Only data that have passed the FINO 1 quality check are considered.[39] A log-normal distribution is fitted to the wind speed dependent turbulence intensity distribution for each year.[62] The 90th percentile value for the turbulence intensity is taken as the design value for each wind speed.[45] A normal distribution is fitted to the yearly design turbulence intensity and taken as input for the sensitivity analysis.

Turbulence intensity clearly demonstrates the difference between considering the short-term variability in an environmental parameter (as marked with "V" in Table 1) and the uncertainty in the design parameter. Figure 4 shows the probability distribution of the 10 min turbulence intensity measurements from FINO1 and the distribution of the 1-year design values. A significant reduction in the uncertainty is seen when considering the latter.

To limit the number of independent variables in the SA, the same percentile is used for the TI in the different wind bins (refer Section 2.1.1). Table 6 gives the distribution parameters for the turbulence intensity.

A power law wind profile is fitted to the measurements using the mean 10-min wind speed at the eight anemometers located from 33 to 100 m above MSL.[63] In addition to the exclusion zone of 0–180° mentioned for the turbulence intensity, data from wind directions between 270° and 360° are excluded from the fitting to avoid shadow effects from the met-mast.[64] Furthermore, data samples with goodness-of-fit (R^2-value) less than 0.75 are excluded. The 1-year mean is taken as the design value for the wind shear.[45] Equation (20) shows the applied power law

TABLE 6 Distribution of design turbulence intensity for each wind bin

Wind speed class (m/s)	Distribution
8–10	N(9.20%, 0.62%)
14–16	N(8.82%, 0.35%)
20–22	N(8.82%, 0.42%)

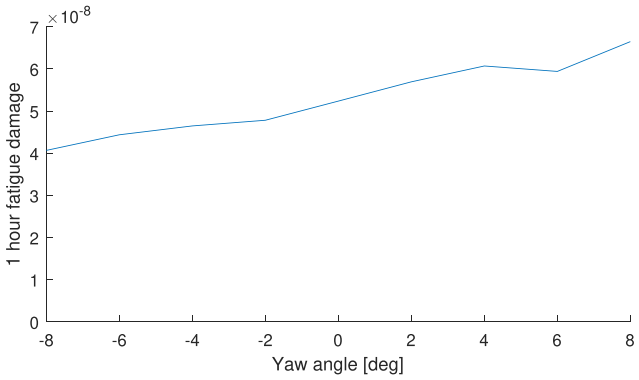

FIGURE 5 Average 1-h fatigue damage in tower base for various yaw angles

formulation, where U is the wind speed at height z and α is the power law exponent. A normal distribution with mean 0.14 and standard deviation 0.01 was fitted to the 1-year mean values of α (Table 3).

$$U(z) = U_{ref}\left(\frac{z}{z_{ref}}\right)^{\alpha}. \tag{20}$$

4.1.4 | Yaw error

Veldkamp[13] assigns a normal distribution with mean 0° and standard deviation 1° to the yaw error. On the other hand, the design codes[1,45] require fatigue analysis to be carried out for yaw misalignments of −8°, 0° and 8°. To avoid increasing the already large computational effort, it was desirable to use only one yaw angle in the simulations. A screening study showed that no single yaw error could predict the correct fatigue damage across the whole support structure. However, the elementary effects method is based on the derivatives of fatigue damage w.r.t. to input parameters. Figure 5 shows the fatigue damage in the tower base of the DTU 10-MW turbine as function of yaw angle, averaged over the wind speeds being used in this study. Although there is a noticeable difference in the fatigue damage at the different yaw angles, the gradient is approximately constant. It was concluded that a single yaw error could be used for the SA. The yaw error was, therefore, modelled using the distribution from Veldkamp.[13]

4.1.5 | Significant wave height and peak period

The wind speed-dependent scatter diagrams of the wave climate are represented by a single lumped sea-state for each wind speed bin. Following the frequency-domain lumping method described by Katsikogiannis et al,[35] one damage-equivalent lumped load case is found for each year of the 60-year NORA10 database.[38] Therefore, for each wind bin, 60 $H_s - T_p$ combinations are found, as shown in Figure 6 for the 14–16 m/s bin. A normal distribution was fitted to the H_s, T_p parameters of the sea-state parameters of the lumped load cases, shown in Table 7. Although Figure 6 strongly suggests there is a correlation between H_s, T_p, this correlation is disregarded to allow assessing the sensitivity of H_s and T_p individually.

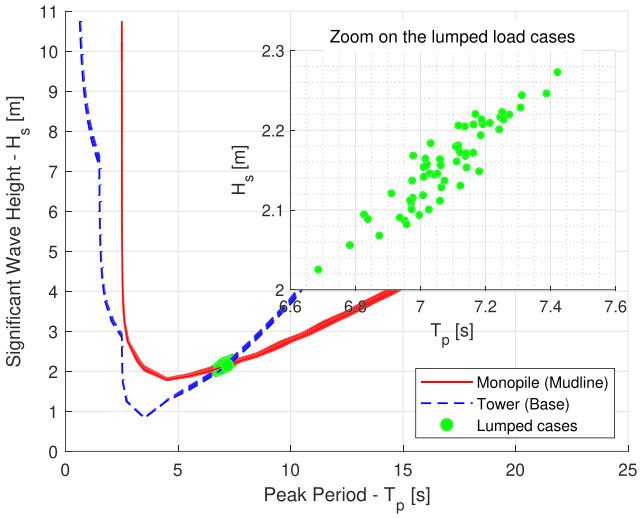

FIGURE 6 Lumped load cases for wind bin 14–16 m/s. Lines represents damage-equivalent sea states for the tower and monopile. The dots give sea states that will reproduce the lifetime fatigue damage in both the tower and monopile. One dot is seen for each year in the NORA10 data set

TABLE 7 Distribution of lumped sea-state parameters H_s, T_p for each wind bin

Wind speed bin (m/s)	5 MW		10 MW		15 MW	
	H_s (m)	T_p (s)	H_s (m)	T_p (s)	H_s (m)	T_p (s)
8–10	N(1.27, 0.03)	N(6.42, 0.11)	N(1.24, 0.05)	N(6.37, 0.15)	N(1.28, 0.03)	N(7.29, 0.15)
14–16	N(2.29, 0.03)	N(7.27, 0.12)	N(2.16, 0.05)	N(7.08, 0.14)	N(2.08, 0.06)	N(7.04, 0.22)
20–22	N(3.73, 0.09)	N(8.48, 0.21)	N(3.49, 0.07)	N(8.24, 0.18)	N(3.36, 0.07)	N(8.13, 0.21)

TABLE 8 Distribution parameters for wind-wave misalignment per wind bin

Wind speed bin (m/s)	Distribution	
	Mean	$\sigma_{\theta_{rel,m}\|U_k}$
8–10	0°	N(47.9°, 2.5°)
14–16	0°	N(24.6°, 3.0°)
20–22	0°	N(15.7°, 2.0°)

4.1.6 | Wind-wave misalignment

The wave directional properties are assumed described by the wind direction and wind-wave misalignment conditional on the wind speed, similar to Horn et al.[48] The misalignment was found to follow a normal distribution, with a mean of 0° for all wind speeds. This gives the standard deviation of the misalignment, $\sigma_{\theta_{rel,m}|U_k}$, as the uncertain parameter. By analysing the NORA10 data, a normal distribution was found to be a reasonable fit for $\sigma_{\theta_{rel,m}|U_k}$. The probability of being in misalignment bin m is given as

$$P^j(\theta_{rel,m}|U_k) = 2\left(\mathrm{F}(\theta_{m,u};0,\sigma^j_{\theta_{rel,m}|U_k}) - \mathrm{F}(\theta_{m,l};0,\sigma^j_{\theta_{rel,m}|U_k})\right). \quad (21)$$

Here, $\mathrm{F}(x;\mu,\sigma)$ denotes the cumulative normal distribution with mean μ and standard deviation σ. $\theta_{m,u}$ and $\theta_{m,l}$ denote the upper and lower limits of the misalignment bin, respectively. $\sigma_{\theta_{rel,m}|U_k}$ is the wind speed dependent standard deviation of the misalignment. The multiplication with 2 assumes that positive and negative misalignment angles can be treated as equal. The properties of the misalignment model are given in Table 8.

4.1.7 | Marine growth and drag coefficient

Marine growth is modelled using the depth varying thickness profile found in GL's standards for offshore wind turbines.[65] The uncertainty is modelled by scaling the marine growth at all depths equally, where the mean value at mean sea level is set to 100 mm.[45] The standard deviation is taken from Jusoh and Wolfram[40] using the coefficient of variation (C.o.V.) for mussels in the Southern North Sea, as mussels are the most prominent growth in shallow waters.[66] A normal distribution is assumed, and the shape of the depth-dependent thickness profile is assumed constant.

The drag coefficient is assumed normally distributed with a mean of 0.7 and a standard deviation of 0.1.[4,13] In principle, there is a relationship between the marine growth and the drag coefficient. However, the drag coefficient depends on the surface roughness of the marine growth, not the thickness.[40] Therefore, the marine growth and drag coefficient are assumed independent of each other in the present study.

4.1.8 | Undrained shear strength and void ratio

The undrained shear strength, s_u, and shear modulus, G_{max}, at small strains are considered the most important uncertainties for the present soil profile. These are included in the study as s_u/σ'_{v0} and void ratio, e, respectively. σ'_{v0} is the vertical effective stress. Laccasse and Nadim[41] assign a normal distribution to s_u/σ'_{v0}, with mean value 1 and a standard deviation in the range 5–15%. The upper limit of 15% has been used here.

The void ratio, e, typically has a coefficient of variation of 7–30%.[41] However, physical bounds linked to e_{min} and e_{max} dictate a coefficient of variation of maximum 8.3% for the assumed soil profile. Therefore, a normal distribution with mean 0.7 and standard deviation 0.058 is assumed.

4.1.9 | Monopile diameter

Zaaijer[42] assumes a variation of $\pm$ 0.1% in the diameter of monopile foundations. Hübler et al[5] translated this to a uniform distribution with upper and lower bound 0.1% from the nominal diameter. The same uncertainty model is used in the present study.

4.1.10 | Fatigue parameters

Consistent with other studies,[4,6] uncertainty in the SN curve (Equation 15) is modelled as uncertainty in the intercept parameter, a, while the negative inverse slope, m, is modelled as deterministic. DNV GL gives the standard deviation in $\log(a_{1,2})$ as 0.2, and states that the design curves are given as the mean minus two standard deviations.[43] This gives the SN-parameters in Table 9 when using suitable design SN curves. In addition to the SN curve parameters, the fatigue capacity Δ_C is modelled as uncertain. This is assumed to follow a lognormal distribution with mean value 1 and standard deviation 0.3.[4,44]

4.1.11 | Availability

Little information is available concerning the availability of individual OWTs over the full lifetime. Design standards[45] consider an availability of 90%,[45] while various sources state average availability of wind farms in the range 85–96%.[46,47] Availability as low as 80.3% for the first three operational years has been reported as an extreme case.[67] Here, a lognormal distribution is assumed for the unavailability (100% - availability). This is done to avoid sampling availability above 100%, corresponding to unavailability below 0%. A mean value of 10% is assumed as indicated by design standards,[45] while the standard deviation is set to 2.5%. The latter corresponds to experience from two wind farms.[46]

TABLE 9 SN curve parameters

Parameter	Type	Tower	Monopile
$\log(a_1)$	Stochastic	N(12.564, 0.2)	N(12.164, 0.2)
$\log(a_2)$	Stochastic	N(16.006, 0.2)	N(16.006, 0.2)
m_1	Deterministic	3	3
m_2	Deterministic	5	5

4.2 | Discrete parameters

Five discrete parameters are considered in the study. The discrete parameters differ from the continuous, as a probability density function cannot be assigned to them. One discrete parameter is changed at a time, with the remaining parameters being kept at the baseline value. The calculations are repeated for all base points in the continuous analysis. A summary of the parameters is given in Table 10, with details given in the following sections. The baseline case corresponds to the modelling choices that were used for analysing the continuous parameters.

4.2.1 | Turbulence and coherence model

The Kaimal turbulence model with exponential coherence and Mann uniform shear turbulence model are compared in the study. These are recommended for design load calculations by IEC 61400-1 4th Ed.[68] In the present study, three models are compared: the Kaimal model with spatial coherence only in longitudinal direction (baseline case), the Kaimal model with spatial coherence in three directions, and the Mann model. The design standard does not provide values of the decrement $(\alpha_{u,v,w})$ and offset $(b_{u,v,w})$ coherence parameters for the lateral (v) and vertical (w) components for the exponential coherence. These are defined similarly as in Wise et al,[69] and variability in these parameters is not considered. Spatial coherence is inherently implemented in the Mann model, and the model parameters are determined based on IEC 61400-1.[68]

4.2.2 | Wave spreading

Traditionally, waves have been modelled as long-crested when performing fatigue analysis on OWTs. This is applied as the baseline model in this study, with the variation being short-crested waves. Short-crested waves are included by multiplying the unidirectional wave spectrum with a spreading function, as recommended by, for example, DNV[70]:

$$S(\omega,\theta;\theta_0) = S(\omega)D(\theta;\theta_p). \tag{22}$$

Here, $S(\omega)$ is the wave spectrum, while $D(\theta;\theta_p)$ is the spreading function with directional components θ and mean wave direction θ_p. The spreading function is modelled as

$$D(\theta;\theta_p) = \frac{\Gamma(1+n/2)}{\sqrt{\pi}\Gamma(1/2+n/2)}\cos^n(\theta-\theta_p), \tag{23}$$

with the spreading exponent n assumed equal to 2 for all sea states.

4.2.3 | Wave spectrum

To evaluate the effect of the wave spectrum, two alternative formulations are compared to the baseline wave spectra (Section 3.5). The first variation is the TMA wave spectrum,[70] which modifies the JONSWAP spectrum to account for finite water depth. This is done by multiplying the original spectrum by a depth function (Equation 24) based on the wave number $k = \omega^2/g \cdot \tanh kd$ and water depth d as shown in Equation (25).[70]

$$S_{TMA}(\omega) = S(\omega) \cdot \phi_{TMA}(\omega). \tag{24}$$

TABLE 10 Discrete parameter variations

Parameter	Baseline	Variations	
Coherence model	Coherence in x-direction	Coherence in x,y,z-directions	Mann model
Wave spreading	Long-crested	Short-crested	
Wave Spectrum	PM/JONSWAP	TMA	Torsethaugen
Soil Model	Macro element	$p-y$ curves	
Scour protection	No	Yes	

$$\phi_{TMA}(\omega) = \frac{\sinh^2(kd)}{\sinh^2(kd) + kd\coth(kd)} \tag{25}$$

The second variation is the Torsethaugen spectrum.[71] This is a two-peaked spectrum applicable in areas where there is an important swell component in addition to wind generated sea. The spectrum was established primarily for one location at the Norwegian Continental Shelf and is completely defined given the total significant wave height and spectral peak period. The model splits the energy into a swell component and wind-sea component, using a modified JONSWAP spectrum for both peaks.

4.2.4 | Soil-structure interaction model

The macro-element model described in Section 3.4 is the baseline soil-structure interaction model. The effect of the soil-structure interaction model has been evaluated by comparing the macro-element model, which incorporates hysteretic damping, against a $p-y$ curve-based beam on spring model. The latter is a more common approach, as these can easily be incorporated in simulation tools for OWTs. In the $p-y$ curves model, the monopile is modelled as a beam below seafloor, and the soil is represented by as a series of discrete, uncoupled elastic springs attached to nodal positions along the pile. Both models are calibrated to the same FEA results. In addition, soil damping is implemented in the monopile of the model using p-y curves as stiffness-proportional Rayleigh damping, tuned by a decay test to give the same damping ratio as the macro element (Section 5.3.2).

4.2.5 | Scour protection

Design calculations on monopile OWTs are typically performed without considering scour protection. To assess how the scour protection influences the response prediction, a 1.5-m-thick protection layer consisting of gravel and rocks was added to the foundation model (Section 3.4). The layer was assumed to be completely drained with a maximum mobilized angle of friction of 50° and an effective unit weight of 12 kN/m^3. For consistency in the results presentation, the seafloor is defined as the top of the original soil layer, i.e. below the scour protection.

5 | RESULTS

This section will present the results of the sensitivity analysis. First, the fatigue utilization from the 30 base points is presented in Section 5.1, before the results of the continuous parameters are given and discussed in Section 5.2. Finally, the results from the discrete parameters are presented in Section 5.3.

5.1 | Fatigue utilization

The fatigue utilization from the variations of the continuous parameters is shown in Figure 7. Grey lines show the results from the 30 different base points, while the black lines show the mean utilization. In the monopile, the fatigue utilization follows the same pattern in all turbines, with maximum fatigue damage 4–6 m below seafloor. The 5- and 10-MW towers both see the highest fatigue utilization in the base. A larger utilization is also seen towards the tower top, due to the rotor tilting moment. The 15-MW tower is optimized for the ultimate limit state.[32] As a result, the tower dimensions are more irregular, giving highest fatigue utilization $\sim$ 20 m below the tower top.

The variation in fatigue utilization among the base points is described by the coefficient of variation (C.o.V.) in Figure 7. This is fairly similar in all turbines, varying between 55% and 67%. All turbines show a slight increase in variability towards the tower top.

The contribution of individual wind speeds to the lifetime fatigue damage is determined by the short-term fatigue damage of each environmental condition and the probability of occurrence for that condition. Figure 8 shows this distribution for tower base and seafloor. The lower wind speeds contribute more to the fatigue damage as the turbine size increases, which is indicative of the wind loads becoming more important.[72] This is verified by considering the ratio between wind loads and wave loads in the three turbines. Assuming the aerodynamic moment at seafloor is given by quasi-static thrust force, F_a, and distance to the hub, z_{hub}, the aerodynamic moment can be written as

$$M_a = F_a z_{hub}. \tag{26}$$

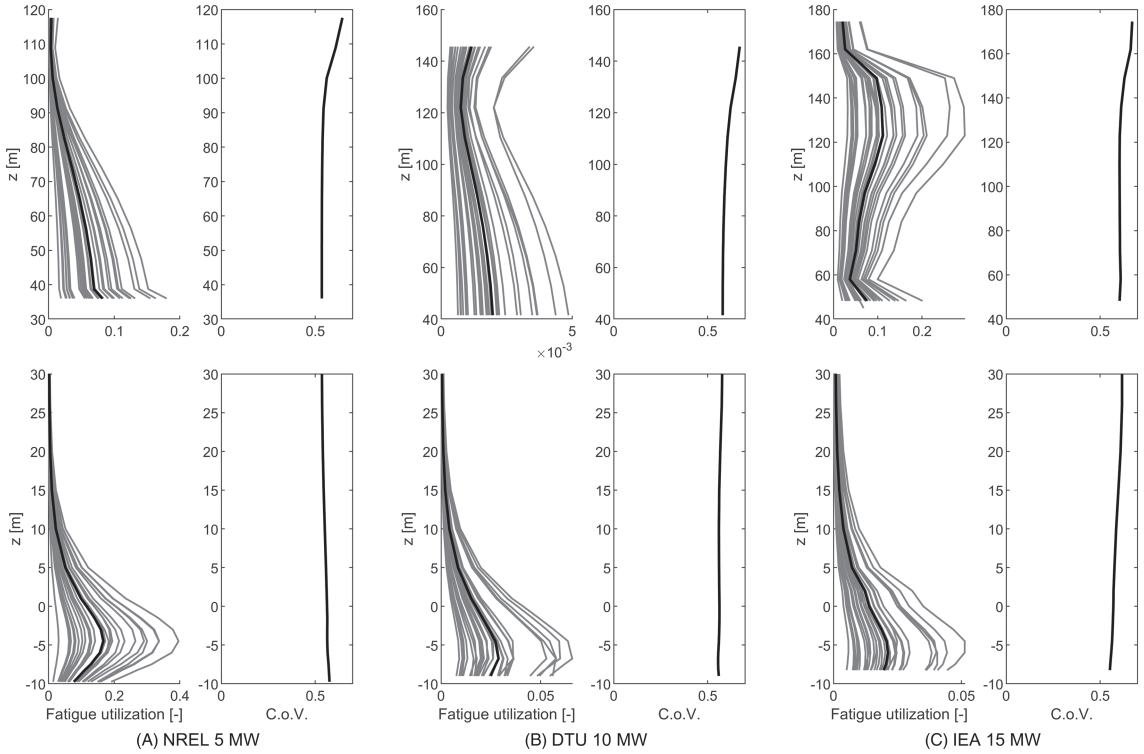

FIGURE 7 Distribution of fatigue utilization and C.o.V. along the monopile and tower. The black line represents the mean of all base points, while grey lines are individual base points. Results in the lower part of the monopile are not shown. Seafloor is at $z = 0$

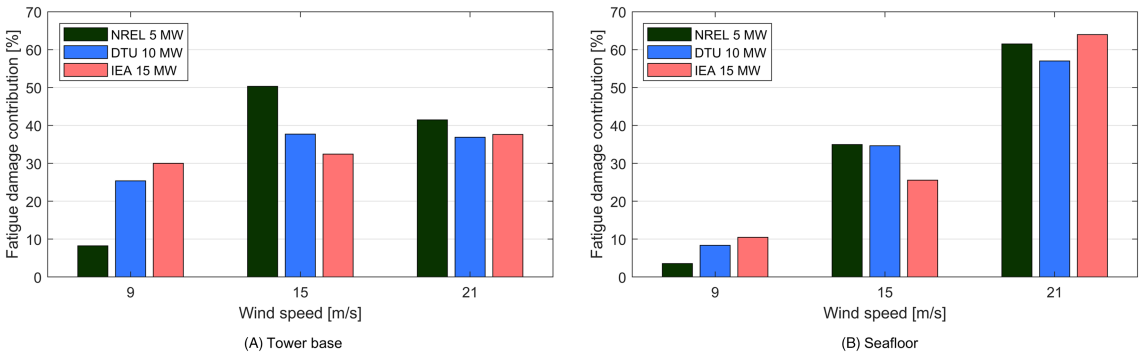

FIGURE 8 Contribution to fatigue utilization from wind speed classes

Similarly, the hydrodynamic moment is proportional to M_h if Morison's equation[73] is applied:

$$M_h = \rho C_m D_p^2 H_s T_p^{-2} h^2. \tag{27}$$

Here, ρ is the density of water, C_m is the mass coefficient equal to 2, D_p is the pile diameter and h is the water depth. Using the mean thrust, H_s and T_p from the wind bin 14–16 m/s in Table 7, the ratio M_a/M_h is approximately 25 for the 5-MW turbine, 35 for the 10-MW turbine and 43 for the 15-MW turbine. This shows that wind loads become more important as the turbine size increases.

Figure 9 shows the contribution from parked and operational conditions to the fatigue damage. It is known that parked conditions contribute significantly to the fatigue damage in monopile-supported OWTs due to the lack of aerodynamic damping and resonant response of the first global mode.[14] This is particularly true in the tower base, where the parked conditions of the 5-MW turbine account for ~ 60% of the fatigue

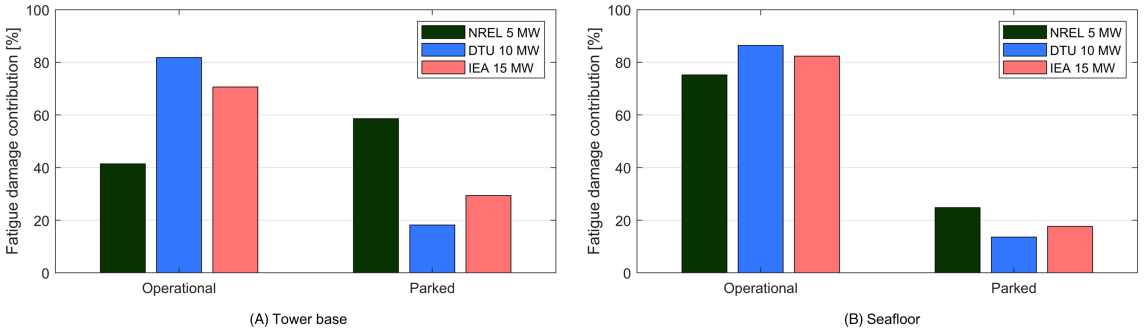

FIGURE 9 Contribution to fatigue utilization from operational and parked conditions

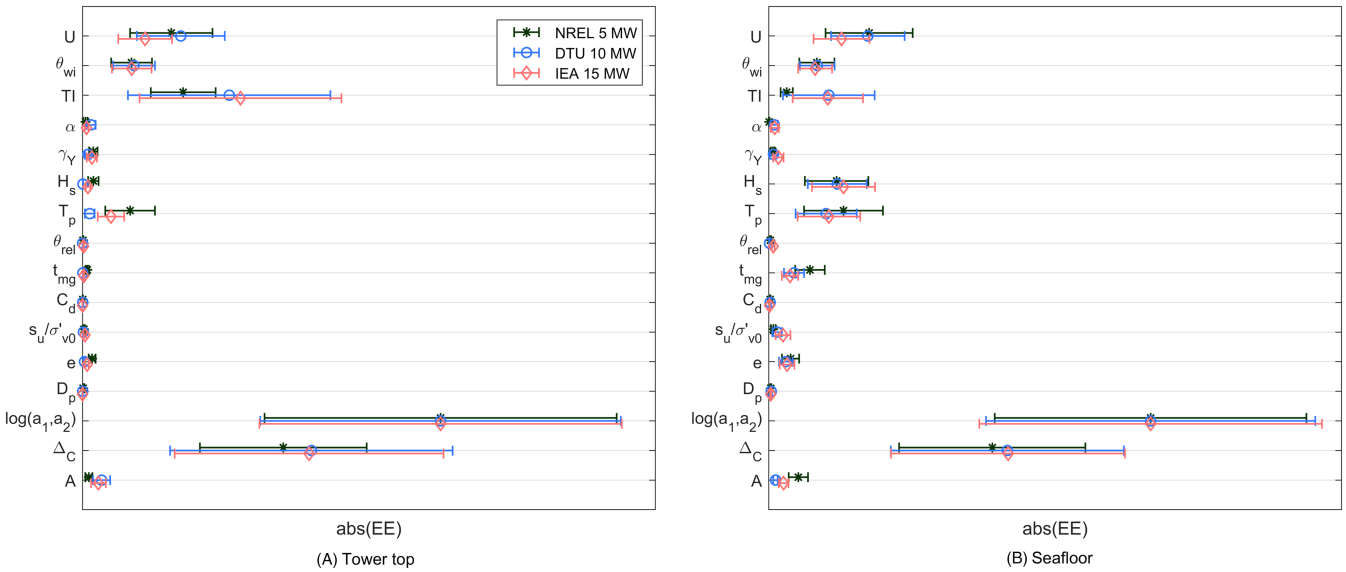

FIGURE 10 Statistics of the elementary effects at tower top and seafloor. The markers represent $\mu^*_{EE,i}$, while the bars show $\pm\sigma_{EE,i}$. All plots are scaled based on the largest mean value for each turbine and location. Confer Table 3 for definition of symbols

damage (Figure 9A). The effect is less pronounced in the larger turbines, where wave loads are less dominating for the response. Parked conditions are also significant in the fatigue utilization of the monopile (seafloor shown in Figure 9B). Only operational conditions contribute significantly to the fatigue damage in the tower top (not shown), as this is dominated by the rotor tilting moment and the generator induced side-side moment.

5.2 | Continuous parameter results

The uncertainty caused by the continuous parameters is evaluated using the absolute mean (μ_i^*) and standard deviation ($\sigma_{EE,i}$) of the elementary effects (Section 2.1). Figure 10 shows the results at the tower top and seafloor, with the tower base and monopile max fatigue showing similar results. The markers represent μ_i^* and the bar widths represent $\sigma_{EE,i}$. For each turbine and location, the values are normalized by the highest μ_i^* for that turbine and location. For all turbines and locations, the SN curve parameters $\log(a_1,a_2)$ have the largest influence on the uncertainty in fatigue utilization. The second-most influential parameter is the fatigue capacity, Δ_C. This is in accordance with the results by Peeringa and Bedon[4] and Velarde et al.[34] However, Velarde et al[6] found fatigue capacity to be the more important of the two. Both Peeringa and Bedon[4] and Velarde et al[6] have found the uncertainty in $\log(a_2)$ to be of far greater importance than $\log(a_1)$. This is due to the fatigue damage mainly being caused by stress cycles in the low-stress range of the SN curves. However, there has been little progress in reducing the uncertainty in fatigue parameters. Already in 1984, Wirsching[74] suggested distributions similar to those used today for both $\log(a_1,a_2)$ and Δ_C. One of the main goals of this paper is to suggest how to reduce uncertainty in the design process. As it is not expected that the uncertainty in the fatigue parameters

can be reduced within a design project, the fatigue parameters are omitted from the remaining results. The variation in $\log(a_1,a_2)$ and Δ_C are still included in the calculations, to capture potential interactions with the remaining parameters. When disregarding the fatigue parameters, the results are shown in Figure 11.

5.2.1 | Tower top

In the tower top, the most influential parameter is the turbulence intensity (TI), followed by wind speed distribution and wind direction distribution. For the 10- and 15-MW turbines the turbulence intensity is the parameter with the highest standard deviation in EE, indicating a significant coupling with other parameters. It should also be noted that with the current environmental model (Section 3.2) the wind speed distribution is not only a measure of the wind speed itself, but rather the severity of the environment at the site. This is caused by the environmental model used, where the H_s and T_p distributions are conditional on the wind class.

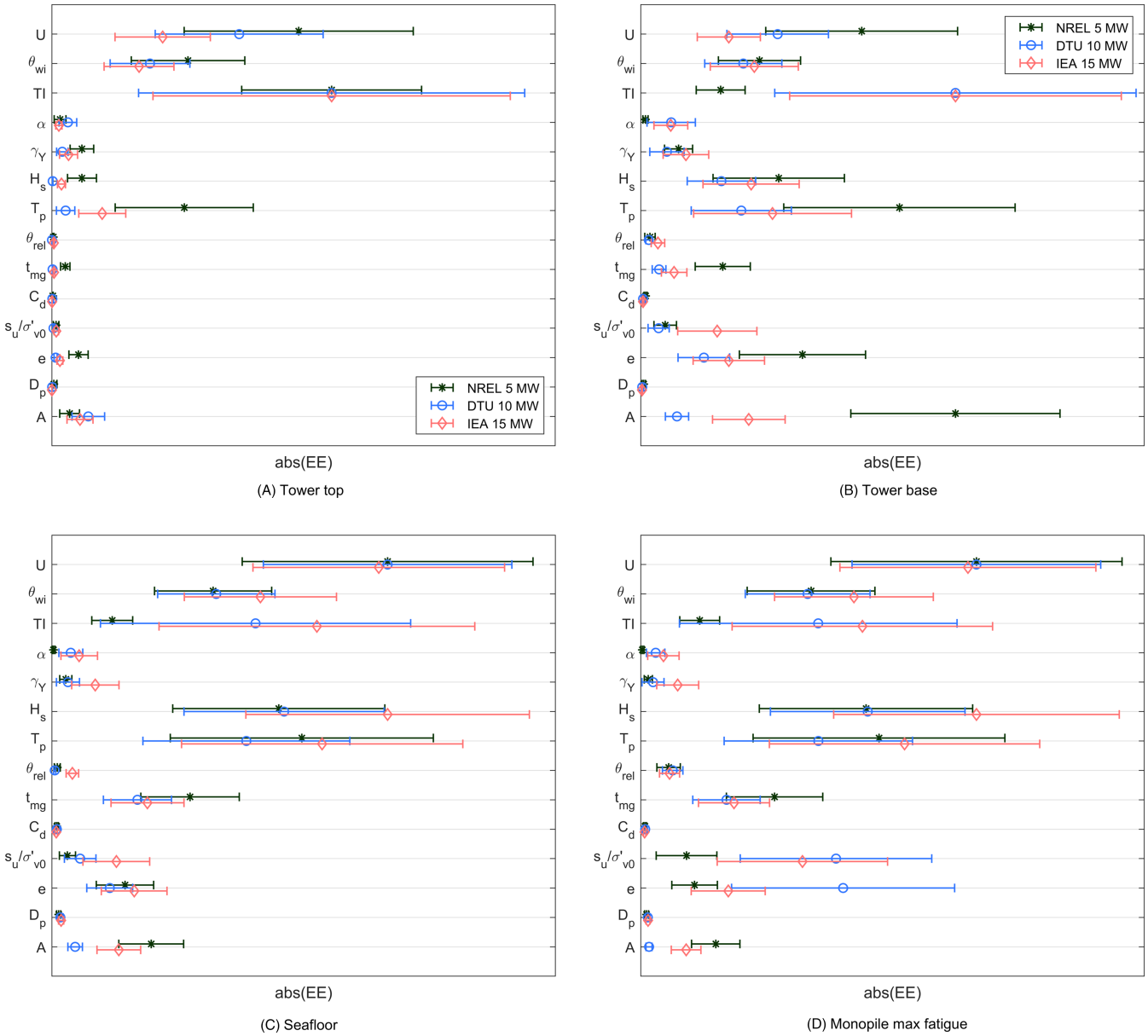

FIGURE 11 Statistics of the elementary effects excluding SN parameters and fatigue capacity. The markers represent $\mu^*_{EE,i}$, while the bars show $\pm\sigma_{EE,i}$. All plots are scaled based on the largest mean value for each turbine and location. Confer Table 3 for definition of symbols

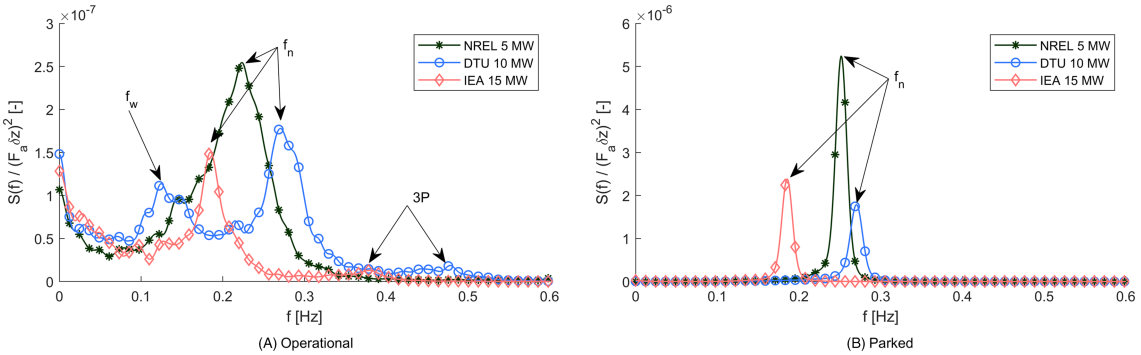

FIGURE 12 Tower base fore-aft bending moment at wind speed 21 m/s, aligned wind and waves. f_n denotes the first fore-aft natural frequency, 3P denotes the blade passing frequency and f_w indicates the wave frequency region

5.2.2 | Tower base

Turbulence intensity dominates the uncertainty also in the tower base for the 10- and 15-MW turbines. For the NREL 5-MW turbine, availability is the dominating parameter followed by wave peak period and wind speed distribution. The difference between the turbines can be explained by how the different turbine states contribute to the fatigue damage (Figure 9). The parked state contributes with about 60% of the fatigue damage in the tower base of the 5-MW turbine, which is two to three times larger than the contribution for the other turbines. Figure 12 shows the fore-aft bending moment at tower base for wind speed 21 m/s in operational and parked conditions, normalized by the steady-state bending moment caused by the thrust at the mean wind speed. In operational conditions, the wave-induced loads show a significantly higher contribution to the response in the 5-MW turbine than for the larger turbines. The higher wave loads are also seen in the increased resonant response in parked conditions, making parked conditions more important for the 5-MW turbine. The dominance of parked response explains the importance of availability for the 5-MW turbine. Further, T_p variation is more important in parked conditions due to the resonant response characteristics, and the wind speed distribution becomes important through the variation of T_p between the wind classes.

Robertson et al.,[9] Teixeira et al[8] and Toft et al[11] focused on the tower response in their studies. They found that turbulence intensity has the highest impact on the fatigue utilization uncertainty, agreeing with the overall results in this study.

5.2.3 | Monopile

The severity of the environmental conditions (represented by wind speed distribution in the used environmental model) is the most influential uncertainty in the monopile, with the uncertainty in H_s within each wind bin being equally important for the 15-MW turbine. The remaining significant parameters illustrate some of the differences between the three turbines. H_s and T_p variations both resulted in significant elementary effects for all turbines, while the importance of the turbulence intensity decreases with decreasing turbine size. The latter is caused by the higher importance of wind loads in the larger turbines.

Hübler et al.,[5] Peeringa and Bedon[4] and Velarde et al[6] have all looked at the monopile in their studies. Of these, only Hübler et al. can be directly compared with the results in this study. They found soil parameters, marine growth thickness, and pile diameter to be the most influential parameters at seafloor for the NREL 5-MW turbine. When considering only the parameters included both by Hübler et al. and the present study, the results seem consistent. Marine growth and soil parameters (void ratio in this study) are the the two most important parameters present in both studies. Structural pile diameter is not found to influence the fatigue utilization in the present study, while turbulence intensity is found more important here. The latter is particularly the case for the larger turbines.

5.3 | Discrete parameter results

The overall results from the analysis of the discrete parameters are shown in Figure 13. The wind coherence model is the most influential parameter in the tower top, with particularly the Mann model giving different results for the 5- and 10-MW turbines when compared to the baseline model. The choice of soil model and wave spectrum has the largest influence on the fatigue damage estimation in the tower base for 5- and 10-MW turbines, together with the inclusion of scour protection for the 5-MW turbine. For the IEA 15-MW turbine, the Mann coherence model also shows a significant difference compared to the baseline model. Scour protection has the highest influence on the fatigue damage estimation

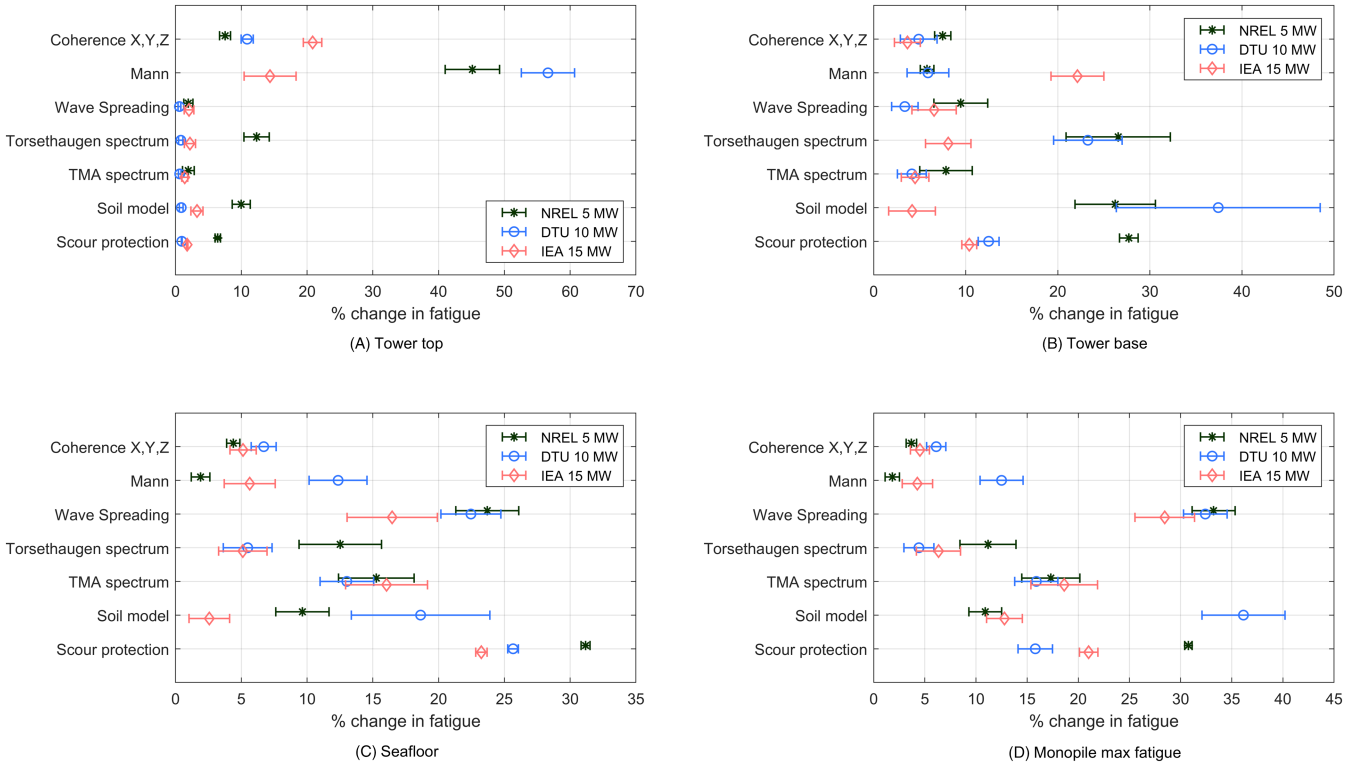

FIGURE 13 Change in fatigue damage when considering alternative models. The markers represent $\mu^*_{\delta D,i}$ while the bars show $\pm\sigma_{\delta D,i}$

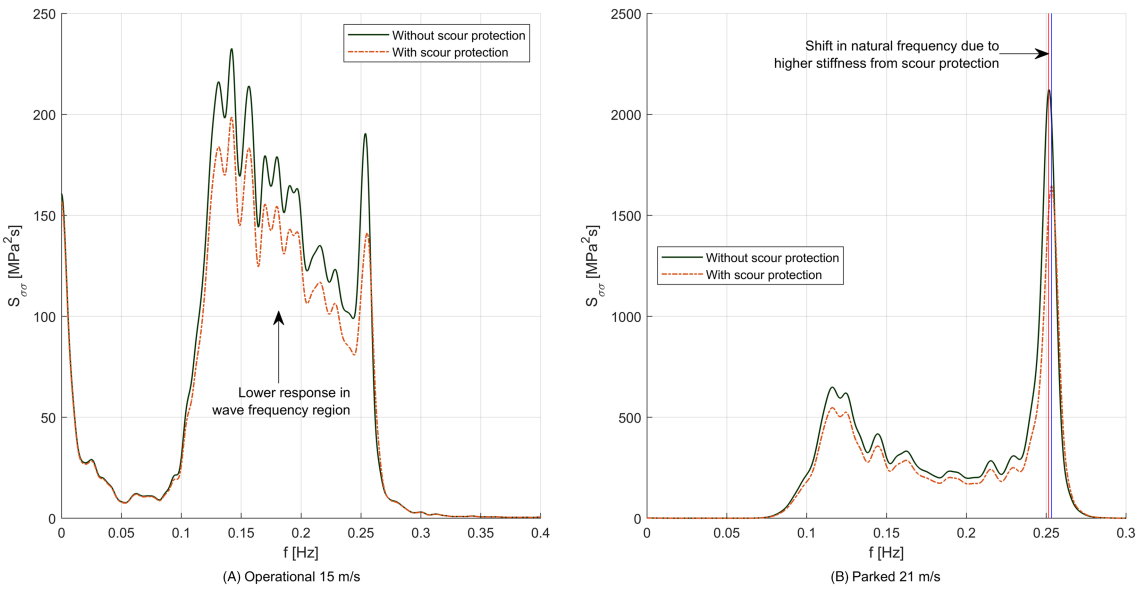

FIGURE 14 Stress spectra for location facing wave direction at seafloor with 30° wind-wave misalignment with and without scour protection modelled for NREL 5-MW turbine

at seafloor, which for consistency is defined as being the intersection between the soil and the scour protection layer. A significant difference is also seen when changing the wave spectral model and soil model, as well as when modelling the waves as short-crested. Finally, wave spreading and the soil model seems to cause the largest changes to the maximum fatigue damage prediction in the monopile. The following sections will present some of the results in more detail.

5.3.1 | Scour protection

The presence of scour protection at seafloor increases the foundation stiffness. This results in lower responses in the wave frequency region, and slightly increases the natural frequency. The latter is evident for conditions with low or negligible aerodynamic damping, e.g. conditions with wind-wave misalignment and when the OWT is parked. Figure 14 shows the stress spectra at seafloor for the 5 MW model. Both cases are with 30° misalignment, in operational and parked conditions. The change in the natural frequency is about 1.5%, 0.5% and 0.3% for the 5, 10 and 15 MW turbines, respectively. This explains the larger change in fatigue damage shown for the 5-MW turbine in Figure 13. Generally, larger variations were found for the parked conditions compared to the operational. Small changes were seen in conditions with wind-wave misalignment.

5.3.2 | Soil modelling

Figure 13 shows a significant difference between the turbines when changing soil model from the macro element formulation to p-y curves. Using the p-y curves leads to three distinct changes in the response, all illustrated in Figure 15 for the DTU 10 MW and IEA 15-MW turbines. First, the soil stiffness is reduced, leading to higher response amplitudes in the wave frequency range. This is because the p-y springs only models the virgin

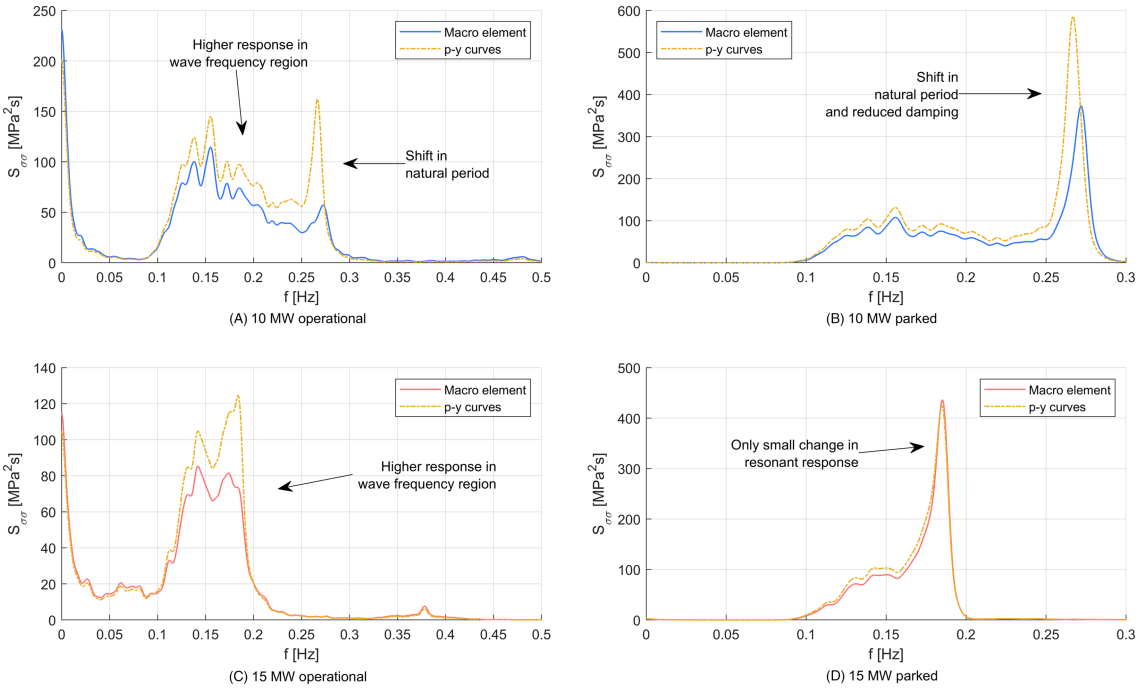

FIGURE 15 Stress spectra in monopile for DTU 10 MW and IEA 15-MW turbines in operational and parked conditions with wind speed 15 m/s

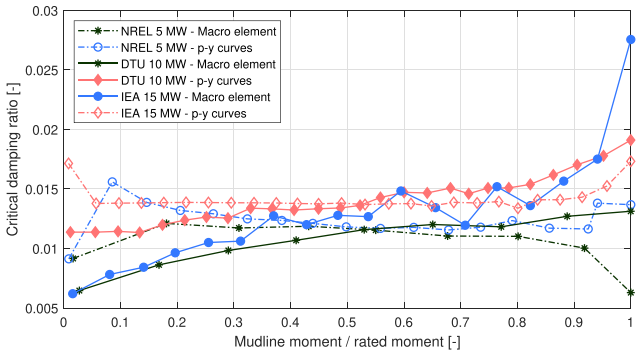

FIGURE 16 Damping ratios when using the macro element and p-y curves as function of seafloor bending moment

stiffness curve, while the macro element captures the unloading reloading stiffness better. Second, the lower soil stiffness gives a lower natural frequency. This effect is larger for the smaller turbines, consistent with what is seen in Section 5.3.1. Finally, the damping level is different when varying the soil models. In Figure 15B and D, it seems like the damping is too low for the 10-MW model with p-y curves, while the damping is more consistent in the 15-MW turbine.

However, the damping level of friction materials as soil is amplitude-dependent. This effect is captured by the macro element approach, as shown in Figure 16. Here, the global damping level is given as function of seafloor bending moment, with the latter normalized by M_a in Equation (26). The effect of the amplitude-dependent damping is that the p-y curves predict a higher resonant response in some wind classes and a lower response in other wind classes when compared to the macro element. For the 15-MW turbine these overpredictions and underpredictions cancel each other for the wind speeds considered in this study. This leads to small differences in the lifetime fatigue damage when considering the different soil models. This is particularly the case in the tower base and at seafloor, where the resonant response is significant. Below seafloor, the response is dominated by the wave-frequencies and the difference between the models is smaller. It is also worth noticing that there is still a significant difference in the short-term response characteristics of the 15-MW turbine when varying the soil model, which here happens to add up to small changes in the lifetime fatigue damage at seafloor and tower base.

6 | DISCUSSION

The results show that the uncertainty in both the continuous and discrete parameters are important for the fatigue damages estimation in monopile OWTs. However, designers and researchers should focus on different parameters.

The following general advice can be given to a designer who wants to reduce the uncertainty in a fatigue analysis: (i) Reduce the uncertainty in the SN curve and fatigue capacity if possible. (ii) Reduce the uncertainty in the environmental design basis, including both wind and wave parameters. Here, the design requirement of 1 year of available data has been used as the design basis. Increasing to two years of data will reduce the standard deviation of the assumed distributions by $\sim$ 30% if the standard deviations are proportional to $1/\sqrt{n}$. Using 5 years of measurement data will reduce the standard deviations by $\sim$ 55%. (iii) Consider carefully which models are appropriate for the discrete parameters. All discrete variations have an influence on some parts of the support structure. However, the soil model seems to be particularly important at both the tower base and for the maximum fatigue damage in the monopile.

It is the discrete parameters (wind coherence model, wave spectral and spreading model, and soil models) that are of highest interest for future research, as the uncertainty in the most important continuous parameters can be reduced by increasing the amount of data available in the design basis. While all variations show importance in some part of the structure, it is worth noticing that most influential parameter for the 15-MW turbine is the wave spreading model. Together with the soil model, this is also the most influential parameter in the monopile for the other turbines. There may also be a coupling between the choice of soil model and the effect of wave spreading, which has not been investigated further here. The cross-wind and parked response of the turbines are sensitive to the soil damping level, as aerodynamic damping is mainly present in the fore-aft direction of an operational turbine. Any cross-wind loading will give a significant response level, which motivates the need to look at either the response at several locations around the circumference of the structure or the long-term response. Despite this, wave spreading has received little attention in the research community, with the authors knowing only three studies.[21,22,75] The effect of the soil model is also significant, demonstrating the need for accurate modelling of soil damping and stiffness. In terms of the coherence model, most models used today are developed for small diameter rotors with onshore wind conditions. Comparisons with measured time series and high-fidelity simulations show the need for further research also in this field.[18]

While this paper investigates both parameter uncertainty (the continuous variables) and model uncertainty (the discrete variables), no direct comparison between the two types of uncertainty has been performed. Both uncertainties contribute to the uncertainty in the design. Future studies could therefore focus on determining the relative importance of these distinctively different sources of uncertainty.

7 | CONCLUSION

This paper has investigated the uncertainty in the fatigue utilization caused by input parameters using fully coupled time-domain analyses. Continuous parameters, which are described by probability density functions, and discrete parameters, describing different engineering models, have been considered. The SN-curve parameters and fatigue capacity were found to be the continuous parameters with the highest influence in the uncertainty. Furthermore, parameters related to the description of the environmental conditions were found important. Generally, wind related parameters were found to be the most important in the tower, while wave related parameters were most important in the monopile. The importance of the wind parameters for the monopile increased with increasing turbine size, suggesting that uncertainties in the wind parameters become more important for the emerging large turbines. All the evaluated discrete parameters had an influence on the uncertainty of fatigue

damage estimates. The most important were found to be the coherence model in the tower top, and the soil model for the monopile at seafloor and tower base. Wave spreading had the highest influence on the maximum fatigue damage in the monopile.

ACKNOWLEDGEMENTS

Part of this work has been carried out at the Centre for Autonomous Marine Operations and Systems (AMOS). The Norwegian Research Council is acknowledged as the main sponsor of NTNU AMOS. This work was supported by the Research Council of Norway through the Centres of Excellence funding scheme, project number 223254 - AMOS. Additionally, the authors gratefully acknowledge the support from the Wave Loads and Soil Support for Extra Large Monopiles (WAS-XL) project (NFR grant 268182). Data were made available by the FINO (Forschungsplattformen in Nord- und Ostsee) initiative, which was funded by the German Federal Ministry of Economic Affairs and Energy (BMWi) on the basis of a decision by the German Bundestag, organised by the Projekttraeger Juelich (PTJ) and coordinated by the German Federal Maritime and Hydrographic Agency (BSH)

PEER REVIEW

The peer review history for this article is available at https://publons.com/publon/10.1002/we.2755.

ORCID

Stian H. Sørum https://orcid.org/0000-0003-1131-5078
George Katsikogiannis https://orcid.org/0000-0002-1137-3764
Erin E. Bachynski-Polić https://orcid.org/0000-0002-1471-8254
Jørgen Amdahl https://orcid.org/0000-0002-3668-9896
Ana M. Page https://orcid.org/0000-0001-9197-0181

REFERENCES

1. IEC. International Electrotechnical Commission, Design Requirements for fixed offshore wind turbines (IEC 61400-3); 2019.
2. DNV GL. DNVGL-ST-0126. Support structures for wind turbines; 2018.
3. Saltelli A, Ratto M, Andres T, et al. Global sensitivity analysis. *The Primer*. Chichester, UK: John Wiley & Sons, Ltd; 2008.
4. Peeringa J, Bedon G. Fully integrated load analysis included in the structural reliability assessment of a monopile supported offshore wind turbine. *Energy Procedia*. 2017;137:255-260. https://doi.org/10.1016/j.egypro.2017.10.348
5. Hübler C, Gebhardt CG, Rolfes R. Hierarchical four-step global sensitivity analysis of offshore wind turbines based on aeroelastic time domain simulations. *Renew Energy*. 2017;111:878-891. https://doi.org/10.1016/j.renene.2017.05.013
6. Velarde J, Kramhøft C, Sørensen JD, Zorzi G. Fatigue reliability of large monopiles for offshore wind turbines. *Int J Fatigue*. 2020;134:105487. https://doi.org/10.1016/j.ijfatigue.2020.105487
7. Haldar S, Sharma J, Basu D. Probabilistic analysis of monopile-supported offshore wind turbine in clay. *Soil Dyn Earthq Eng*. 2018;105:171-183. https://doi.org/10.1016/j.soildyn.2017.11.028
8. Teixeira R, O'Connor A, Nogal M. Probabilistic sensitivity analysis of offshore wind turbines using a transformed Kullback-Leibler divergence. *Struct Saf*. 2019;81:101860. https://doi.org/10.1016/j.strusafe.2019.03.007
9. Robertson AN, Shaler K, Sethuraman L, Jonkman J. Sensitivity analysis of the effect of wind characteristics and turbine properties on wind turbine loads. *Wind Energ Sci*. 2019;4(3):479-513. https://doi.org/10.5194/wes-4-479-2019
10. Ziegler L, Muskulus M. Fatigue reassessment for lifetime extension of offshore wind monopile substructures. *J Phys Conf Ser*. 2016;753(9):092010.
11. Toft HS, Svenningsen L, Sørensen JD, Moser W, Thøgersen ML. Uncertainty in wind climate parameters and their influence on wind turbine fatigue loads. *Renew Energy*. 2016;90:352-361. https://doi.org/10.1016/j.renene.2016.01.010
12. Kallehave D, Byrne BW, LeBlanc Thilsted C, Mikkelsen KK. Optimization of monopiles for offshore wind turbines. *Philos Trans R Soc A Math Phys Eng Sci*. 2015;373(2035):20140100.
13. Veldkamp HF. Chances in wind energy: a probalistic approach to wind turbine fatigue design. *Thesis*. Delft, NL; 2006.
14. Damgaard M, Andersen LV, Ibsen LB, Toft HS, Sørensen JD. A probabilistic analysis of the dynamic response of monopile foundations: soil variability and its consequences. *Probabilistic Eng Mech*. 2015;41:46-59. https://doi.org/10.1016/j.probengmech.2015.05.001
15. Negro V, López-Gutiérrez J-S, Esteban MD, Matutano C. Uncertainties in the design of support structures and foundations for offshore wind turbines. *Renew Energy*. 2014;63:125-132. https://doi.org/10.1016/j.renene.2013.08.041
16. Luengo J, Negro V, García-Barba J, López-Gutiérrez J-S, Esteban MD. New detected uncertainties in the design of foundations for offshore wind turbines. *Renew Energy*. 2019;131:667-677. https://doi.org/10.1016/j.renene.2018.07.103
17. Kim S-H, Shin H-K, Joo Y-C, Kim K-H. A study of the wake effects on the wind characteristics and fatigue loads for the turbines in a wind farm. *Renew Energy*. 2015;74:536-543. https://doi.org/10.1016/j.renene.2014.08.054
18. Nybø A, Nielsen FG, Godvik M. Quasi-static response of a bottom-fixed wind turbine subject to various incident wind fields. *Wind Energy*. 2021;24(12):1482-500. https://doi.org/10.1002/we.2642
19. Horn J-TH, Krokstad JR, Amdahl J. Hydro-elastic contributions to fatigue damage on a large monopile. *Energy Procedia*. 2016;94:102-114. https://doi.org/10.1016/j.egypro.2016.09.203
20. Schloer S, Bredmose H, Bingham HB, Larsen TJ. Effects from fully nonlinear irregular wave forcing on the fatigue life of an offshore wind turbine and its monopile foundation. In: Proceedings of the ASME 2012 31st International Conference on Ocean, Offshore and Arctic Engineering American Society of Mechanical Engineers; 2012; Rio de Janeiro, Brazil.

21. Horn J-T, Krokstad JR, Amdahl J. Long-term fatigue damage sensitivity to wave directionality in extra-large monopile foundations. *Proc Inst Mech Eng Part M: J Eng Marit Environ*. 2018;232(1):37-49. https://doi.org/10.1177/1475090217727136
22. Sørum SH, Krokstad JR, Amdahl J. Wind-wave directional effects on fatigue of bottom-fixed offshore wind turbine. *J Phys Conf Ser*. 2019;1356:012011. https://doi.org/10.1088/1742-6596/1356/1/012011
23. Bachynski EE, Ormberg H. Hydrodynamic modeling of large-diameter bottom-fixed offshore wind turbines. In: Proceedings of the ASME 2015 34th International Conference on Ocean, Offshore and Arctic Engineering American Society of Mechanical Engineers; 2015; St. John's, Newfoundland, Canada.
24. Aasen S, Page AM, Skjolden Skau K, Nygaard TA. Effect of foundation modelling on the fatigue lifetime of a monopile-based offshore wind turbine. *Wind Energ Sci*. 2017;2(2):361-376.
25. Katsikogiannis G, Bachynski EE, Page AM. Fatigue sensitivity to foundation modelling in different operational states for the DTU 10mw monopile-based offshore wind turbine. *J Phys Conf Ser*. 2019;1356:012019. https://doi.org/10.1088/1742-6596/1356/1/012019
26. Campolongo F, Saltelli A, Cariboni J. From screening to quantitative sensitivity analysis. a unified approach. *Comput Phys Commun*. 2011;182:978-988.
27. Jansen MJW. Analysis of variance designs for model output. *Comput Phys Commun*. 1999;117(1):35-43.
28. Kucherenko S, Albrecht D, Saltelli A. Exploring multi-dimensional spaces: A comparison of latin hypercube and quasi monte carlo sampling techniques. arXiv preprint arXiv:1505.02350; 2015.
29. Wang R, Diwekar U, Grégoire Padró CE. Efficient sampling techniques for uncertainties in risk analysis. *Environ Prog*. 2004;23(2):141-157.
30. Jonkman J, Butterfield S, Musial W, Scott G. Definition of a 5MW reference wind turbine for offshore system development. *Report*, Denver, CO, US, National Renewable Energy Laboratory (NREL); 2009.
31. Bak C, Zahle F, Bitsche R, et al. Description of the DTU 10 MW reference wind turbine. *Report*, Kgs. Lyngby, DK, DTU Wind Energy; 2013.
32. Gaertner E, Rinker J, Sethuraman L, et al. Definition of the IEA 15-megawatt offshore reference wind turbine, Denver, CO, US, International Energy Agency; 2020.
33. Jonkman J, Musial W. Offshore code comparison collaboration (OC3) for IEA task 23 offshore wind technology and deployment. *Report*, Golden, Colorado, USA, NREL; 2010.
34. Velarde J, Bachynski EE. Design and fatigue analysis of monopile foundations to support the DTU 10 MW offshore wind turbine. *Energy Procedia*. 2017;137:3-13. https://doi.org/10.1016/j.egypro.2017.10.330
35. Katsikogiannis G, Sørum SH, Bachynski EE, Amdahl J. Environmental lumping for efficient fatigue assessment of large-diameter monopile wind turbines. *Mar Struct*. 2021;77:102939.
36. Hansen MH, Henriksen LC. Basic DTU wind energy controller. *Report*, Roskilde, Denmark, DTU Wind Energy; 2013.
37. NREL. ROSCO. Version 2.2.0. https://github.com/NREL/rosco; 2020.
38. Reistad M, Breivik O, Haakenstad H, Aarnes OJ, Furevik BR, Bidlot JR. A high-resolution hindcast of wind and waves for the North Sea, the Norwegian Sea, and the Barents Sea. *J Geophys Res Oceans*. 2011;116(C5):C05019.
39. Bundesamt für Seeschifffahrt und Hydrographie. Fino - datenbankinformationen. https://www.bsh.de/DE/THEMEN/Beobachtungssysteme/Messnetz-MARNET/FINO/fino_node.html; 2020.
40. Jusoh I, Wolfram J. Effects of marine growth and hydrodynamic loading on offshore structures. *Jurnal Mekanikal*. 1996;1(1).
41. Lacasse S, Nadim F. Uncertainties in characterising soil properties. In: Uncertainty in the geologic environment: from theory to practice American Society of Civil Engineers; 1996; Madison, Wisconsin.
42. Zaaijer MB. Foundation modelling to assess dynamic behaviour of offshore wind turbines. *Appl Ocean Res*. 2006;28(1):45-57. https://doi.org/10.1016/j.apor.2006.03.004
43. DNV-GL (Det Norske Veritas - Germanischer Lloyd). Fatigue design of offshore steel structures (DNVGL-RP-C203).
44. Folsø R, Otto S, Parmentier G. Reliability-based calibration of fatigue design guidelines for ship structures. *Mar Struct*. 2002;15(6):627-651. https://doi.org/10.1016/S0951-8339(01)00031-4
45. DNV-GL (Det Norske Veritas - Germanischer Lloyd). Loads and site conditions for wind turbines (DNVGL-ST-0437); 2016.
46. Pfaffel S, Faulstich S, Rohrig K. Performance and reliability of wind turbines: a review. *Energies*. 2017;10(11):1904.
47. Larsen J, Soerensen H, Christiansen E, Naef S. Experiences from Middelgrunden 40 MW offshore wind farm Copenhagen Offshore Wind; 2005; Copenhagen.
48. Horn J-TH, Krokstad JR, Amdahl J. Joint probability distribution of environmental conditions for design of offshore wind turbines Proceedings of the ASME 2017 36th International Conference on Ocean, Offshore and Arctic Engineering; 2017; Trondheim, Norway.
49. SINTEF Ocean. Simo 4.10.3 user guide, Trondheim, Norway, SINTEF Ocean; 2017.
50. SINTEF Ocean. Riflex 4.10.3 user guide, Trondheim, Norway, SINTEF Ocean; 2017.
51. Jonkman BJ. TurbSim user's guide: Version 1.50, Technical Report, Denver, CO, US, National Renewable Energy Lab (NREL); 2009.
52. Larsen HMA. How 2 HAWC2, the user's manual. edited by the DTU wind energy HAWC2 development team, Roskilde, DK, Risø National Laboratory, Technical University of Denmark; 2020.
53. Correia A. A Pile-head Macro-element Approach to Seismic Design of Monoshaft Supported Bridges. *Ph.D. Thesis*. Pavia, Italy: European School for Advanced Studies in Reduction of Seismic Risk, ROSE School; 2011.
54. Page AM, Skau KS, Jostad HP, Eiksund GR. A new foundation model for integrated analyses of monopile-based offshore wind turbines. *Energy Procedia*. 2017;137:100-107. https://doi.org/10.1016/j.egypro.2017.10.337
55. Page A, Grimstad G, Eiksund G, Jostad HP. A macro-element pile foundation model for integrated analyses of monopile based offshore wind turbines. *Ocean Engineering*. 2018; Vol. 167:23-35.
56. Page A, Grimstad G, Eiksund G, Jostad HP. A macro-element model for multidirectional cyclic lateral loading of monopiles in clay. *Comput Geotech*. 2019;106:314-326.
57. Klinkvort RT, Sturm H, Page AM, Zhang Y, Jostad HP. A consistent, rigorous and super-fast monopile design approach Proceedings of the 4th International Symposium on Frontiers in Offshore Geotechnics; 2022; Austin, Texas, US.
58. Burton T, Jenkins N, Sharpe D, Bossanyi E. *Wind Energy Handbook*: John Wiley & Sons, Ltd; 2011.
59. MacCamy R.C., FRA. Wave Forces on Piles: A Diffraction Theory, Washington, D.C., US, Office of Naval Research, U. S. Department of the Navy; 1954.

60. Brodtkorb PA, Johannesson P, Lindgren G, Rychlik I, Rydén J, Sjö E. WAFO—a Matlab toolbox for the analysis of random waves and loads The 10th International Offshore and Polar Engineering Conference; 2000; Seattle, Washington.
61. Masseran N, Razali AM, Ibrahim K, Latif MT. Fitting a mixture of von Mises distributions in order to model data on wind direction in Peninsular Malaysia. *Energy Convers Manag*. 2013;72:94-102.
62. Larsen GC. Offshore fatigue design turbulence. *Wind Energy*. 2001;4(3):107-120. https://doi.org/10.1002/we.49
63. Ernst B, Seume JR. Investigation of site-specific wind field parameters and their effect on loads of offshore wind turbines. *Energies*. 2012;5(10):3835-3855.
64. Türk M, Emeis S. The dependence of offshore turbulence intensity on wind speed. *J Wind Eng Ind Aerodyn*. 2010;98(8):466-471. https://doi.org/10.1016/j.jweia.2010.02.005
65. Germanishcer Lloyd Industrial Services GmbH. Rules and guidelines, IV industrial services, 2 guideline for the certification of offshore wind turbines; 2012.
66. Wolfram J, Theophanatos A. The effects of marine fouling on the fluid loading of cylinders: some experimental results 17th Annual Offshore Technology Conference; 1985; Houston, Texas.
67. Feng Y, Tavner PJ, Long H. Early experiences with uk round 1 offshore wind farms. *Energy*. 2010;163. https://doi.org/10.1680/ener.2010.163.4.167
68. IEC. International Electrotechnical Commission, Wind turbine generator systems-Part 1: Safety requirements. 4th edition (IEC 61400-1); 2019.
69. Wise AS, Bachynski EE. Wake meandering effects on floating wind turbines. *Wind Energy*. 2020;23(5):1266-1285. https://doi.org/10.1002/we.2485
70. DNV-GL. Det Norske Veritas - Germanischer Lloyd, Environmental conditions and environmental loads (DNVGL-RP-C205); 2017.
71. Torsethaugen K, Haver S. Simplified double peak spectral model for ocean waves The Fourteenth International Offshore and Polar Engineering Conference; 2004; Toulon, France.
72. Smilden E, Bachynski EE, Sørensen AJ. Key contributors to lifetime accumulated fatigue damage in an offshore wind turbine support structure Proceedings of the ASME 2017 36th International Conference on Ocean, Offshore and Arctic Engineering; 2017; Trondheim, Norway.
73. Faltinsen OM. *Sea Loads on Ships and Offshore Structures*. Cambridge: Cambridge University Press; 1990.
74. Wirsching PH. Fatigue reliability for offshore structures. *J Struct Eng*. 1984;110(10):2340-2356.
75. Trumars JMV, Jonsson JO, Bergdahl L. The effect of wind and wave misalignment on the response of a wind turbine at Bockstigen Proceedings of the ASME 2006 25th International Conference on Offshore Mechanics and Arctic Engineering; 2010; Shanghai, China.

How to cite this article: Sørum SH, Katsikogiannis G, Bachynski-Polić EE, Amdahl J, Page AM, Klinkvort RT. Fatigue design sensitivities of large monopile offshore wind turbines. *Wind Energy*. 2022;25(10):1684-1709. doi:10.1002/we.2755